Sakurai's Object

A rapidly evolving star

A thesis

submitted in partial fulfilment

of the requirements for the Degree

of

Masters of Science in Astronomy

in the

University of Canterbury

by

Sarah M Wheaton

University of Canterbury

1998

To Mum and Dad,

for their support and encouragement
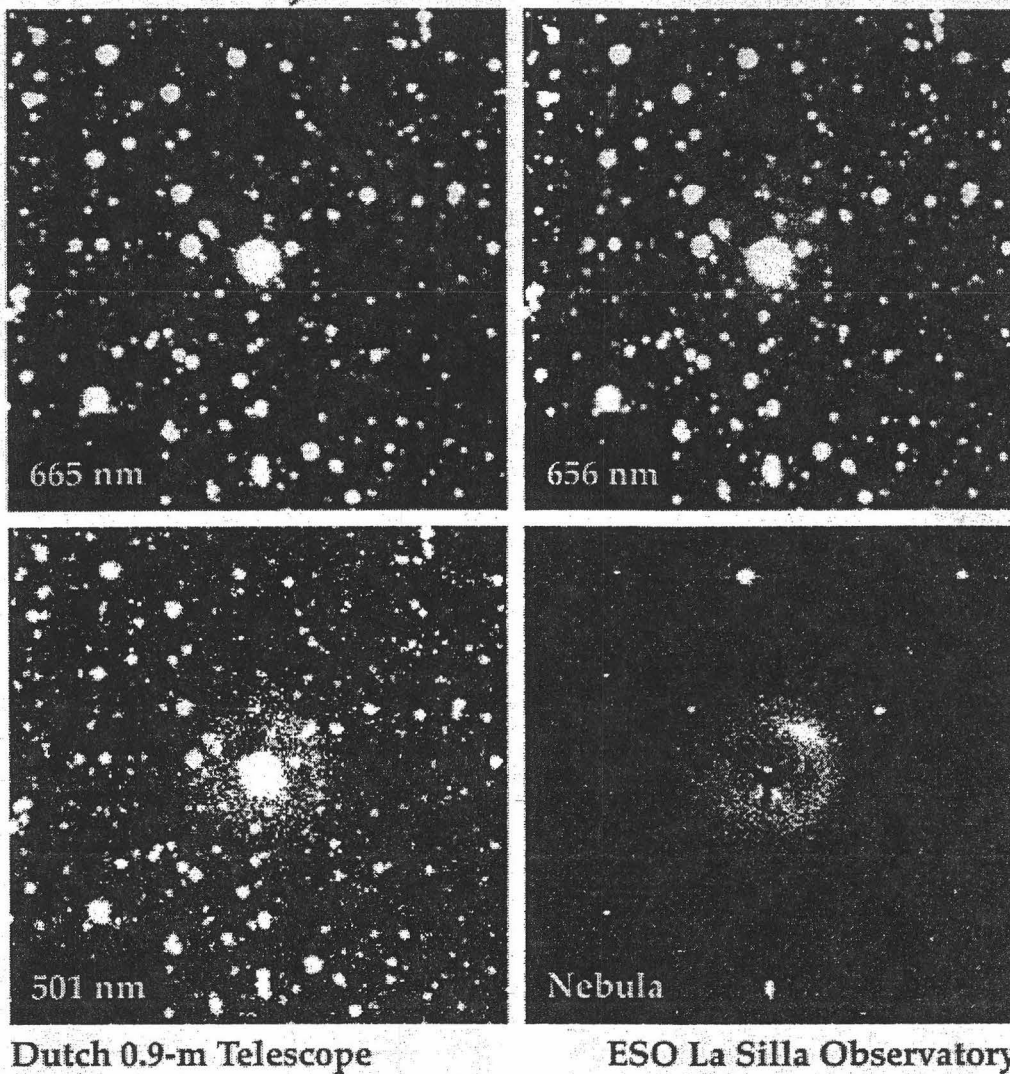over the last twenty-five years.

Figure 1: These CCD images show Sakurai's new star and the planetary nebula surrounding it. The images were obtained with the CCD Camera at the Dutch 0.9-metre telescope at the ESO La Silla Observatory by Hilmar Duerbeck (European Southern Observatory).

Abstract

Sakurai's Object provides an exciting opportunity to study stellar evolution in real time.

This rapidly evolving star discovered in early 1996 by Yukio Sakurai has been observed throughout 1997, and photometric observations are available for 1996. During this period it decreased in temperature from 7800K to 5200K, and increased in luminosity by a factor of 4. The temperature became low enough for a significant amount of carbon containing molecules to form and the star's spectral type changed from a G supergiant to a C-R3 supergiant.

The change in temperature and luminosity is consistent with the object expanding from $40R_\odot$ to $200R_\odot$.

The temperature and luminosity calculated for a distance of 8kpc locate Sakurai's Object at the coolest extent of the final flash evolutionary track for a $0.6\ M_\odot$ planetary nebula nucleus.

At the end of the 1997 observing season Sakurai's Object was still increasing in luminosity. It is expected that eventually this increase will cease and the object will evolve at constant luminosity back to higher temperatures.

Contents

Contents   ix

Contents

Figures

Tables

Chapter 1

Introduction

1.1 What is Sakurai's Object

Sakurai's Object (V4334 Sagittarii) was discovered in early 1996 by Yukio Sakurai, a Japanese amateur astronomer, while doing photographic searches for novae. For him, it was "an unexpected present from the sky, on my birthday". Brightening by $\sim$ 5 magnitudes in less than two years, it provides a unique opportunity to observe stellar evolution on a human timescale.

Sakurai's Object is a candidate for a final helium flash (FF) star. Only two other stars, FG Sagittae and V605 Aquilae have been observed during this phase in the past. The FF scenario has been proposed as a means of formation of at least some R Coronae Borealis (RCB) stars, which are characterised by being hydrogen deficient and carbon rich.

1.1.1 The photometric prehistory of Sakurai's Object

The photometric history of Sakurai's Object is a brief but exciting one [1]. After its discovery on 1996 February 20 various pre-discovery observations were found. A star of $m_j \approx 21$ is seen to coincide with the position of Sakurai's Object on the J plate (blue) of the ESO/SERC sky survey, while the R plate (red), with a plate limit of 20.5, shows no object. Photographic pre-discovery observations reported by Takamizawa show a possible detection at $m_p = 15.5$ in mid 1994, and a rise from $m_p=12.4$ to $m_p=11.2$ between February and October 1995.

1.2 The final flash scenario

Some planetary nebulae nuclei (PNN) may undergo a final flash after having started on the white dwarf cooling sequence. Iben *et al* [2] have shown that in such stars most of the hydrogen is mixed into the convective, helium burning shell and consumed. This is followed by a rapid expansion to red giant dimensions and a $\sim$ 10 000 year long helium burning phase, during which the star retraces the same path on the H-R diagram that it followed during the initial excitation of the nebula. As the star evolves it again reaches a high enough

temperature to brighten the existing planetary nebula (PN). The evolutionary path of a FF star is shown in figure 1.1. Iben *et al* estimated the time for the star to brighten to be $\sim$ 100 years for a star of 0.6 $M_\odot$ and then another $\sim$ 600 years to reach the point where it is hot enough to re-illuminate the PN.
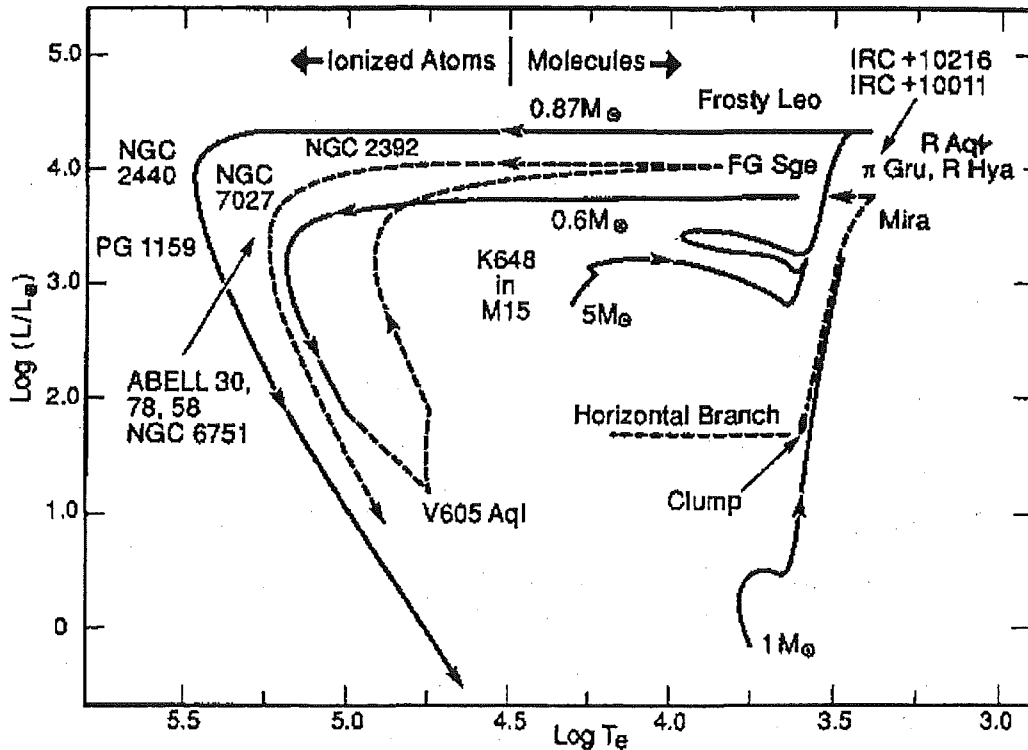
Figure 1.1: This diagram shows the evolutionary track of a 5 $M_\odot$ star which **does not** undergo a final helium flash, and a 1$M_\odot$ star which **does**. The post-helium flash track is marked with the dashed line. Both of these objects loose mass, and the new masses are marked on the evolutionary tracks. Also marked are a number of objects, at different stages in their evolution, including those discussed in the text. This figure is from the review paper by Iben.[3]

1.3 Previously observed final flash objects

FG Sagittae was discovered in 1894, at $m_{pg} = 13.6$ and reached a maximum brightness of $m_B = 9.6$ in 1965. Recent visual estimates have been around 9.5 mag. During the period from 1992 to 1997 FG Sge underwent a series of something like 5 RCB-like declines in brightness, during which spectroscopy showed emission in the C_2 bands and a blue shifted component in the Na D lines, consistent with RCB observations [4]. The light curve during this time (see figure 1.2) is extremely reminiscent of that of the RCB star V854 Cen in figure 1.3. The spectral type has also changed, from B5Ia in 1955 through
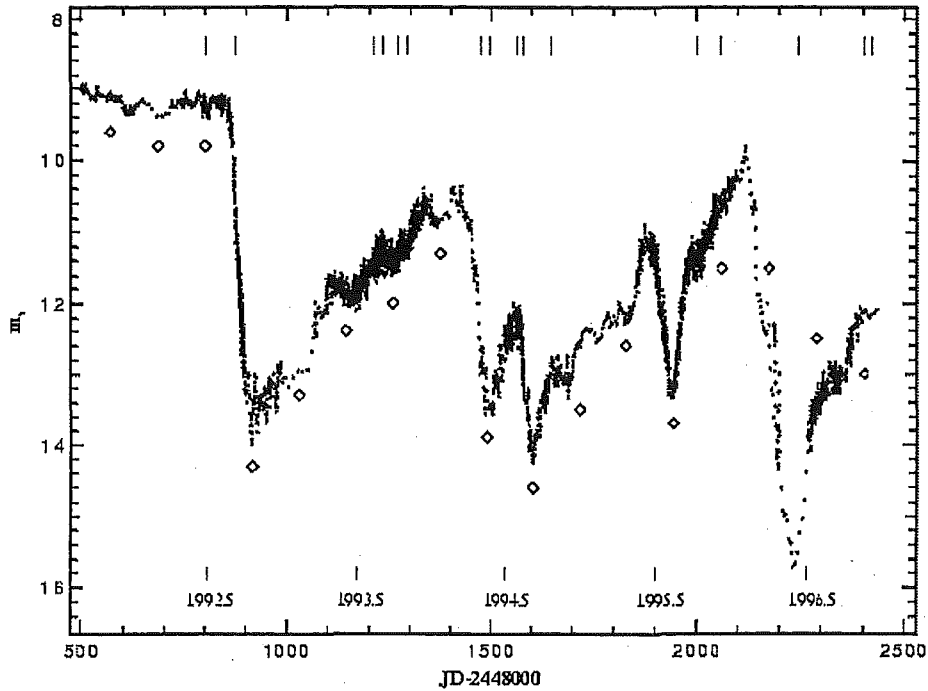
Figure 1.2: The photometric light curve of FG Sge between JD 2448500 and 2450500, showing declines in brightness similar to those of the RCB stars. (Figure from Gonzalez et al. [4])

A5Ia in 1967, G2Ia in the mid 1970s and back to F6 in 1986, where it has remained fairly constant.[1]

V605 Aquilae, which was discovered in 1919, brightened far more rapidly to maximum, from $m_{pg} \simeq 15$ to $m_{pg} \simeq 10.2$ in only about 2 years, a timescale similar to that of Sakurai's Object. Between 1919 and 1923 it declined and recovered three times, this irregular variability thought to be due to dust. It disappeared in 1923, this disappearance also the result of massive dust formation near the surface of the star. A spectrum obtained in 1921 [5] is very similar to that of Sakurai's Object in 1997.

In 1971 V605 Aquilae was found to coincide with the centre of the large PN, Abell 58 [5]. Subsequent imaging shows not only this PN, but a small knot of nebulosity at its geometrical centre. The outer nebula is typical for a PN, except that Hα is weaker than [NII]. The inner nebulosity is rich in helium and deficient in hydrogen.

Harrison [6] shows that the flux from the bright infrared source that V605 Aquilae has since become can be well described using two black body curves (figure 1.4). The far infrared wavelengths fit a black body with a temperature of 150 K, while the visual and near infrared wavelengths fit a black body of

---

[1]Most RCB stars are F or G supergiants
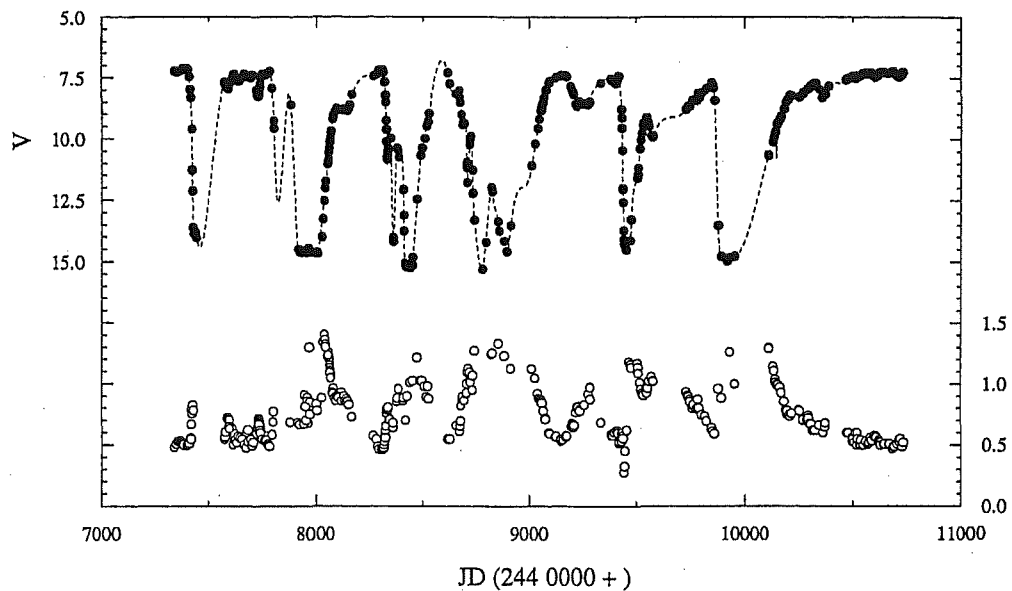
Figure 1.3: The V light curve and $(B\text{-}V)$ colour curve of V854 Cen, an RCB star. This light curve shows frequent declines of the sort typical of RCB stars. (Figure obtained from P.L. Cottrell, private communication.)

50 000 K, reddened by nine magnitudes in the V passband $(A_V = 9)$. Models between 10 000 K with $A_V = 7.9$ and 80 000 K with $A_V = 9.4$ give fits with similar residuals. This implies a shell of dust heated from within by a hot star.

Recent spectroscopic observations [5] show a broad emission feature at 5800 Å which is identified as a stellar C IV line. This feature implies a Wolf-Rayet type, or a weak emission line, spectrum for the central star. In either case, if C IV dominates the spectrum, the central star's temperature must be greater than 50 000 K, which fits nicely with Harrison's infrared photometry findings above.

1.4   Planetary Nebulae

In addition to these examples of a final flash in progress there are two other PNNs which may be the remnants of final flash events.

The nuclei of planetary nebulae Abell 30 and Abell 78 have been identified as being in the post flash helium burning phase. The nebulae have very large radii as would be expected for old, cool nuclei, but the nuclei themselves have high luminosities more characteristic of much younger PNNs. In addition, these two also show evidence of the recent loss of helium-rich material from the surface of their central stars. This material is showing up in the form of resolvable knots of nebulosity at the centres of the old planetary nebulae. The central stars themselves are also completely obscured by dust, observable only
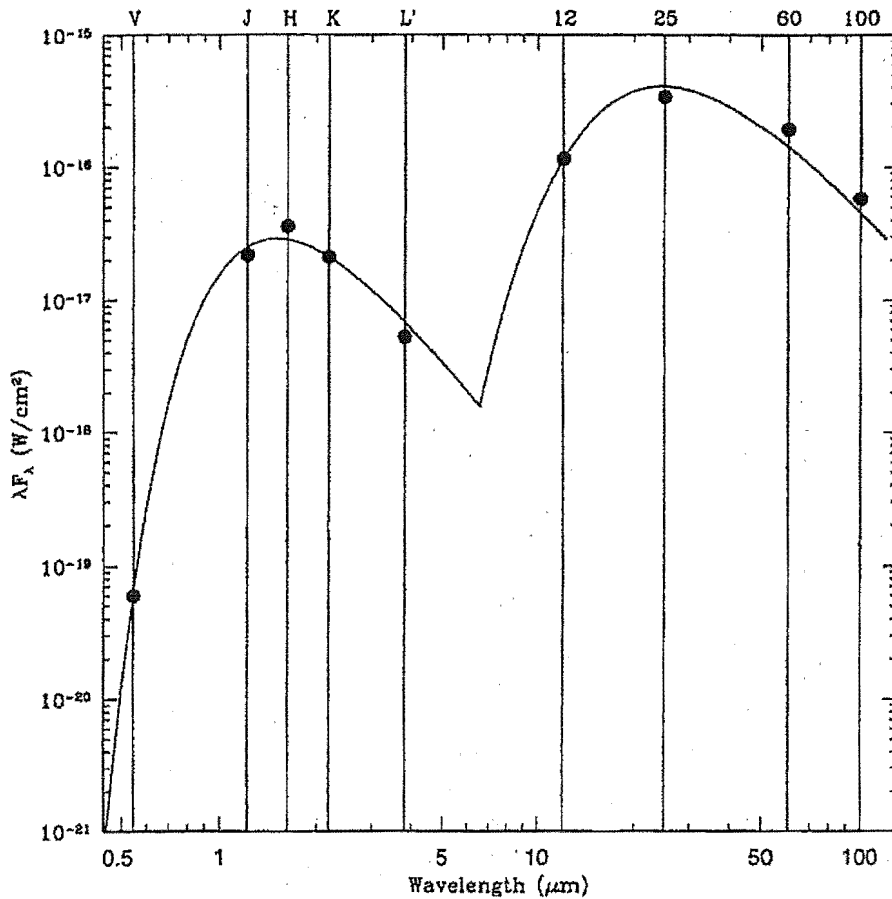
Figure 1.4: Infrared photometry of V605 Aquilae. The photometry is fitted to two black body curves, one of 150K the other of a heavily reddened 50 000K. Figure adapted from fig.3 of Harrison.[6]

as infrared sources.

1.5 Observing Sakurai's Object

The actual observation of an object during a final flash is seen to be a rare and relatively short lived occurrence, and it is important to obtain as many observations of Sakurai's Object as possible to drive further theoretical investigation into this interesting stage of stellar evolution.

Photometric and spectroscopic observations have been made of Sakurai's Object at Mt John University Observatory (MJUO) (Chapter 2). These observations have been reduced and together with previously published data used to derive the physical characteristics of the object during 1996 and 1997 (Chapters 3 and 4).

These physical characteristics have been compared to the existing theoretical models of the final flash phase and to the characteristics of the other

possible final flash stars (Chapters 4 and 5).

Chapter 2

Observations

2.1 Photometry

Photometry of Sakurai's Object commenced at MJUO in 1997 March . Observations were made using the *VBRI* filters similar to those described by Bessell [7] with an EMI 9202B photomultiplier tube and the 0.6m Optical Craftsman telescope. Observations in the U passband were initially attempted, but abandoned after the object proved to be too faint in that passband for it to be worthwhile. The observations were made differentially with respect to a nearby comparison star. The position of the comparison star used, along with the two check stars are shown in figure 2.1 and tabulated in table 2.1.

The differential magnitudes of the variable and two check stars were then transformed to the standard system using coefficients determined from observations of E-Region standards [8]. This reduction to standard magnitudes was done at MJUO using software written by Alan Gilmore.

Each observation was taken twice and the mean of the observations is used. Check star observations are used to determine the consistency of the observations from night to night. The standard deviation of the V observations is 0.04mag, while that of the *B-V*, *V-R*, and *V-I* colours are all 0.03mag. The observations are tabulated in table 2.2 and are plotted in figure 2.2. The point at JD 2 450 532 is brighter and has lower colours than the points immediately surrounding it. The observation report indicates a full moon on the night in question, but no other reason to exclude this point, although it is possible that the wrong star was observed.

In 1997 Duerbeck *et al* [9] published a large amount of *UBVRi* photometric

	R.A.	Dec	V	$(B\text{-}V)$
Sakurai's Object (+)	$17^h52^m33^s$	$-17°41'08''$		
Comparison (C)	$17^h53^m17^s$	$-17°29'02''$	8.25	+1.29
Check (K)	$17^h53^m59^s$	$-17°24'45''$	8.36	+1.81
Star 5	$17^h53^m38^s$	$-17°43'53''$	9.8	+1.35

Table 2.1: The coordinates of Sakurai's Object, the comparison and two check stars.
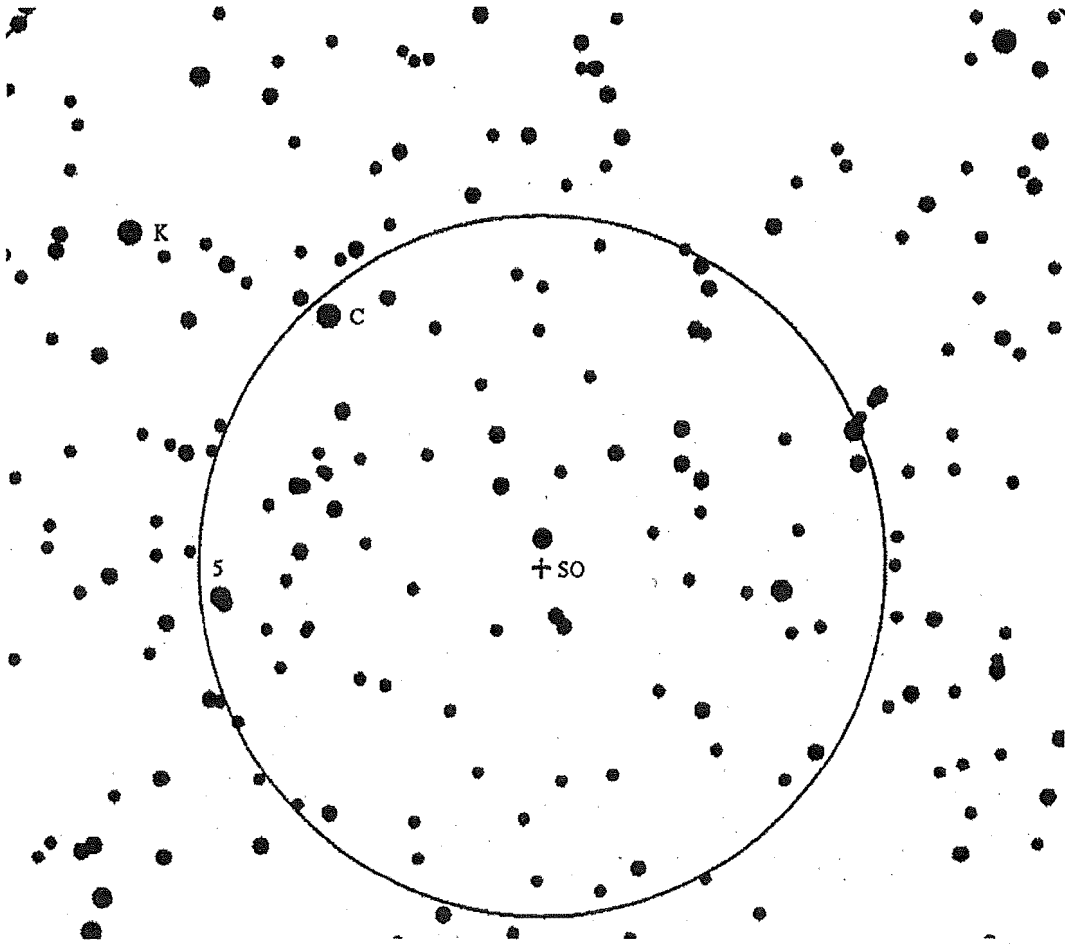
Figure 2.1: Sakurai's Object (+) and the comparison (C) and check stars (K and 5) used in the MJUO photometric program. For scale, the circle is 18' in radius.

data gathered during the 1996 season. Sakurai's Object was measured daily during two observing runs on the Dutch 0.91m telescope at La Silla. Additional observations were also obtained from W. Liller, using a CCD camera and a broad band filter at his observatory in Chile and from C. Nitschelm, using a 7-colour Geneva photometer on the 0.7m Swiss telescope at La Silla. This additional photometry is plotted in figure 2.3 along with the MJUO measurements.

Visual magnitude estimates of Sakurai's Object have been made available by Albert Jones. Initially these estimates were adjusted by -0.23 mag to conform with the MJUO V magnitudes, this being the difference in average magnitude over the period in which these datasets overlap. However they compare well with the photometric measurements from Duerbeck et al without any adjustment at all (see figure 2.4).

It is interesting to note that when compared to photometry published by Duerbeck et al [9], the estimates increase and decrease at the same time, but
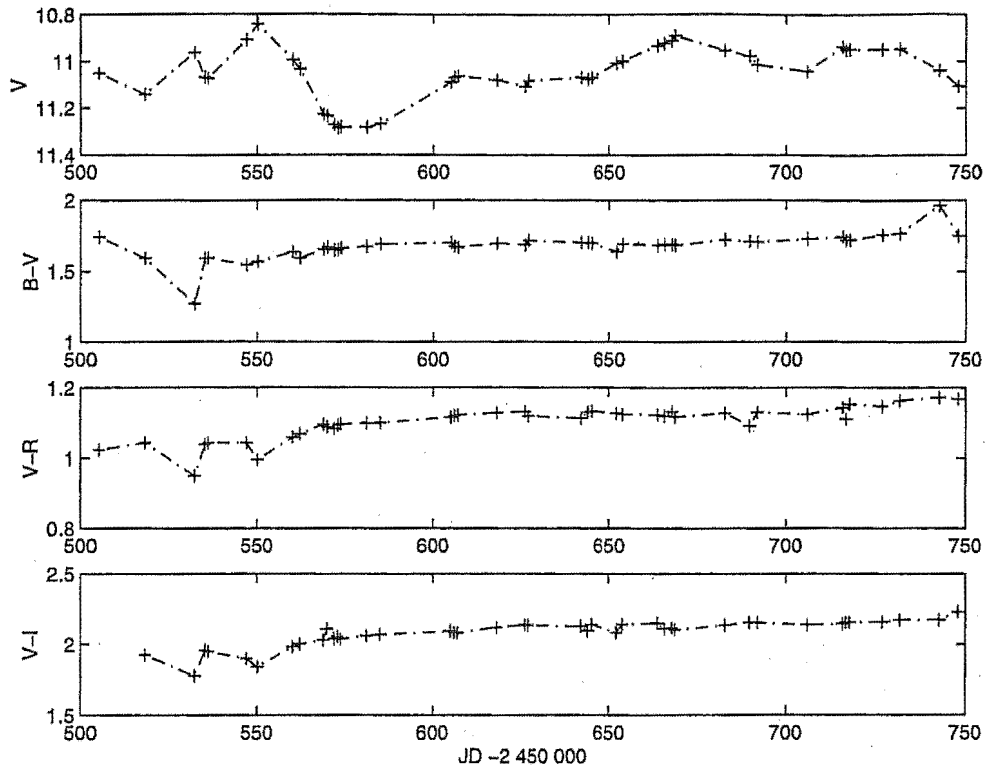
Figure 2.2: Multicolour photometry of Sakurai's Object from MJUO during 1997.

with a larger amplitude.

As all the spectroscopic and photometric evidence indicates that Sakurai's Object has become significantly redder between the end of the 1996 observing season and the beginning of the 1997 observations, there is the possibility that the difference between the visual estimates and the photometric measurements is due to a colour effect. Perhaps Mr Jones' eyes are less sensitive in the red than the *V* filter/photomultiplier tube combination.

These observations all indicate that Sakurai's Object reached its maximum visual magnitude around the end of 1996, but the exact time at which this occurred is uncertain.
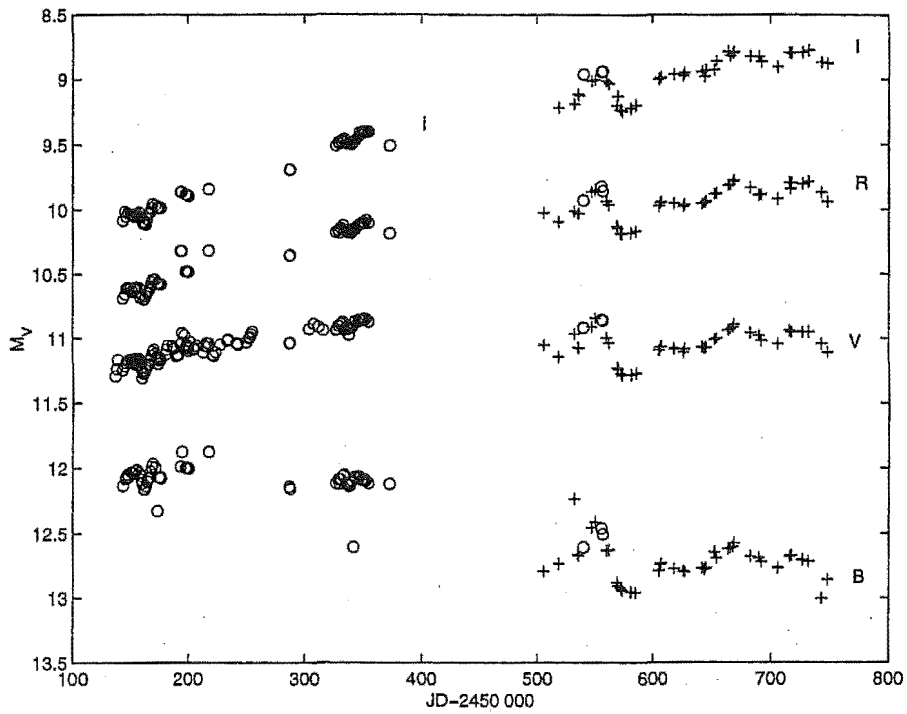
Figure 2.3: All of the photometry available for 1996 and 1997 from Duerbeck *et al* (○) and MJUO (+).
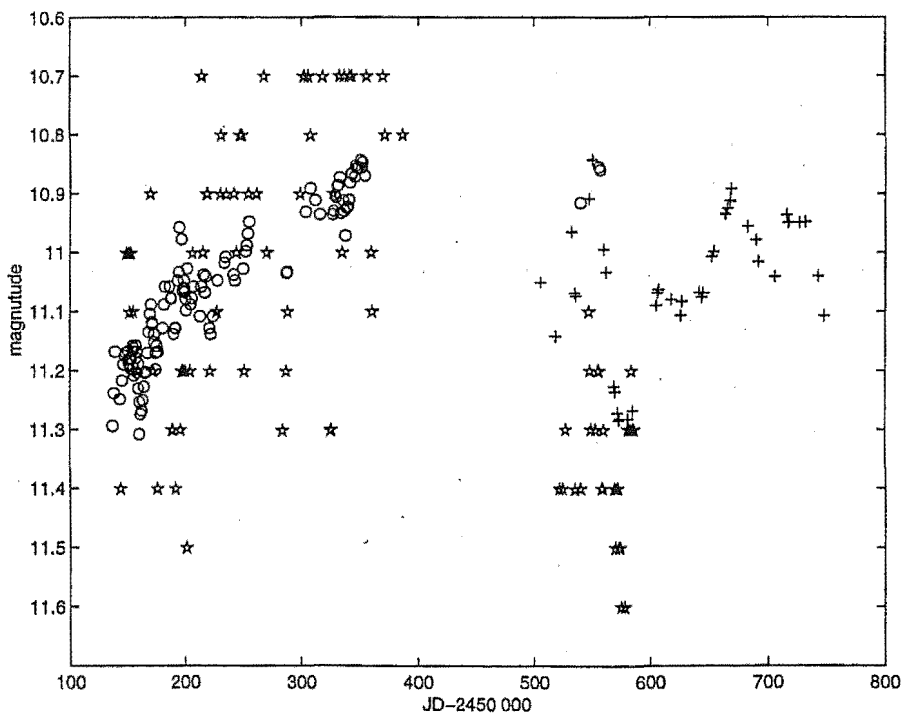
Figure 2.4: All of the *V* photometry available for 1996 and 1997 from Duerbeck *et al* (○) and MJUO (+). Also plotted are the visual estimates made by Albert Jones (⋆), with no offset.

JD-2 450 000	V	U-B	B-V	V-R	V-I	JD-2 450 000	V	U-B	B-V	V-R	V-I
0505.1632	11.051		1.743	1.023		0605.0308	11.090		1.699	1.116	2.093
0518.1827	11.142	0.718	1.591	1.044	1.925	0606.0483	11.069		1.673	1.120	2.082
0532.1974	10.965		1.269	0.950	1.777	0607.0306	11.064		1.668	1.122	2.080
0535.1735	11.069		1.592	1.039	1.956	0618.0407	11.080		1.695	1.128	2.120
0536.1766	11.074	0.308	1.594	1.044	1.950	0625.9945	11.107		1.685	1.132	2.137
0547.1082	10.909		1.544	1.044	1.898	0626.9468	11.083		1.714	1.119	2.135
0550.1357	10.843		1.568	0.996	1.840	0642.0406	11.068		1.700	1.113	2.127
0560.2496	10.995		1.635	1.059	1.981	0643.9843	11.076		1.700	1.130	2.098
0562.2373	11.034		1.592	1.069	2.001	0645.0583	11.069		1.696	1.133	2.140
0569.0521	11.227	0.957	1.653	1.095	2.028	0652.1641	11.007		1.637	1.127	2.083
0570.0641	11.236		1.669	1.088	2.107	0653.8762	10.999		1.691	1.124	2.140
0572.1222	11.272		1.647	1.084	2.040	0663.8594	10.935		1.683	1.123	2.150
0573.1402	11.285		1.649	1.093	2.054	0665.9308	10.925		1.686	1.119	2.110
0573.9932	11.282		1.662	1.096	2.037	0668.0400	10.913		1.689	1.132	2.118
0581.2312	11.282		1.673	1.099	2.061	0668.9736	10.892		1.683	1.117	2.104
0585.1160	11.268		1.690	1.100	2.070						

Table 2.2: Photometric observations of Sakurai's Object made during 1997 at MJUO.

2.2 Spectroscopy

The spectroscopic observations were made with the Medium Resolution Spectrograph (MRS) on the 1m telescope at MJUO. The spectrograph was used with three different gratings and two filters. All of the spectra have been obtained using a slit of 150μm by 30 mm, which corresponds to 2.3 × 460 arc seconds on the sky. This long slit option allows sky subtraction to be performed during the reduction procedure.

The different filters, orders and gratings used and an indication of the resolutions achieved are shown in table 2.3. These pseudo-resolutions were determined by measuring the 1 σ values of lines in the arc spectra and then dividing a typical wavelength near the center of the region studied with that particular region by the 1 σ value. The 1 σ values showed no obvious systematic variation across the width of the chip. The different grating settings used and the wavelength regions obtained in individual observations are in table 2.4. A typical spectrum is shown in figure 2.5.

The detector was a 384× 576 pixel Thomson CCD chip in a liquid nitrogen cooled dewar. The CCD and associated hardware and software were produced by Photometrics Ltd. A helium-argon comparison lamp was used for wavelength calibration and a tungsten halogen lamp for flat fielding.

Filter	Order	Grating	Pseudo-resolution, λ/σ
Schott BG12, 2mm	3	150 l/mm	1600
	3	300 l/mm	3300
	3	600 l/mm	6600
Schott GG475, 2mm	2	150 l/mm	1500
	2	300 l/mm	3100
	2	600 l/mm	6300

Table 2.3: Medium Resolution Spectroscope approximate resolutions with different filters and gratings.

The first spectra were obtained towards the end of 1996 by Ljiljana Skuljan. The spectroscopic observations have continued throughout 1997 until Sakurai's Object was too close to the Sun. Unfortunately, no spectra at the highest resolution (600 l mm^{-1}) were made until after the seasonal break and no high resolution spectra could be taken using the blue (BG12) filter after the break due to the faintness of the object in the blue wavelengths. This is unfortunate in that this is the region most often used for the determination of spectral type.

date	JD-2 450 000	λ from	to	noise	grating	filter	tilt	comments
27/9/96	353.5	5600	6800	4%	300	GG475	255	
27/9/96	353.5	3800	4500	28%	300	BG12	255	Too few counts
28/9/96	354.5	5000	7300	2%	150	GG475	35	
30/9/96	356.5	3700	4500	10%	300	BG12	255	
30/9/96	356.5	5700	6800	4%	300	GG475	255	
9/10/96	365.5	5700	6800	4%	300	GG475	255	
								Seasonal Break
10/3/97	517.5	5700	6800	4%	300	GG475	255	
12/3/97	519.5	5000	7300	2%	150	GG475	35	
14/3/97	521.5	5700	6300	8%	600	GG475	660	This is the first of the highest resolution spectra.
6/4/97	544.5	5610	6300	4%	300	GG475	210	
8/4/97	546.5	5700	6300	8%	600	GG475	660	
1/5/97	569.5	4600	5250	2.5%	600	GG475	580	
2/5/97	570.5	6200	6800	3%	600	GG475	740	
2/5/97	570.5	7100	7700	4%	600	GG475	870	
3/5/97	571.5	5200	5800	5%	600	GG475	580	
3/5/97	571.5	5700	6300	8%	600	GG475	660	
3/5/97	571.5	6200	6800	4%	600	GG475	740	
4/5/97	572.5	7100	7700	4%	600	GG475	870	
4/5/97	572.5	3500	4800	6%	150	BG12	35	No counts below 3900 Å
4/5/97	572.5	5000	7300	2%	150	GG475	35	
6/6/97	605.5	5700	6300	4%	600	GG475	660	
3/8/97	663.5	5000	7300	2%	150	GG475	35	
3/8/97	663.5	3500	4800	16%	150	BG12	35	
3/8/97	663.5	5610	6300	4%	300	GG475	210	
3/8/97	663.5	5700	6800	2%	300	GG475	255	OK
13/9/97	700.5	5000	7300	2%	150	GG475	35	
13/9/97	700.5	5100	6150	5%	300	GG475	210	Problems with
13/9/97	700.5	5700	6800	4%	300	GG475	255	bright moon
13/9/97	700.5	6400	7400	4%	300	GG475	300	and clouds
14/9/97	701.5	5700	6300	?	600	GG475	660	Moon, no clouds

Table 2.4: Spectroscopic observations of Sakurai's Object

Wavelength Angstroms
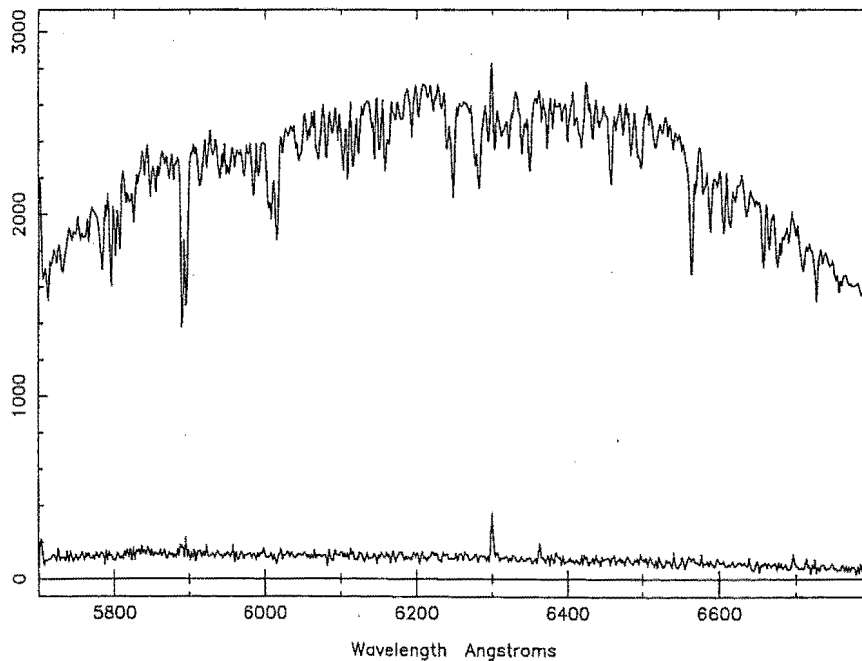
Figure 2.5: An example of a partially reduced MRS spectrum. This spectrum has been wavelength calibrated, but not continuum fitted or sky-subtracted. The sky spectrum is also plotted and shows sky emission lines at 6300 Å and 6365Å. This spectrum was obtained on 1996 September 27 with the 300 l mm^{-1} grating and the GG475 filter.

The spectra obtained throughout the 1997 observing season have not shown any significant changes since the molecular bands appeared during the 1996/97 seasonal break. For a comparison to figure 2.5 see figure 3.1, a 1997 spectrum.

2.3 Colours from low resolution spectra

Spectroscopic observations were obtained late in 1996, but photometric monitoring at MJUO did not start until the 1997 season. Before the publication of Duerbeck *et al*'s [9] photometric data for 1996 there was no colour information available, although visual brightness estimates were available. Information about the colour of the object was needed in order to estimate its temperature. This section describes how a reasonable *(V-R)* colour estimate was found from low resolution spectra.

Using the lowest resolution (150 l mm^{-1}) grating in the second order with the yellow (GG475) filter gives a spectrum covering the wavelength region from 5000 Å to 7300 Å. This wavelength region coincides fairly well with the bandpasses of both the Cousins (see Bessell [7]) V and R filters which were used for the MJUO photometry (see figure 2.6).
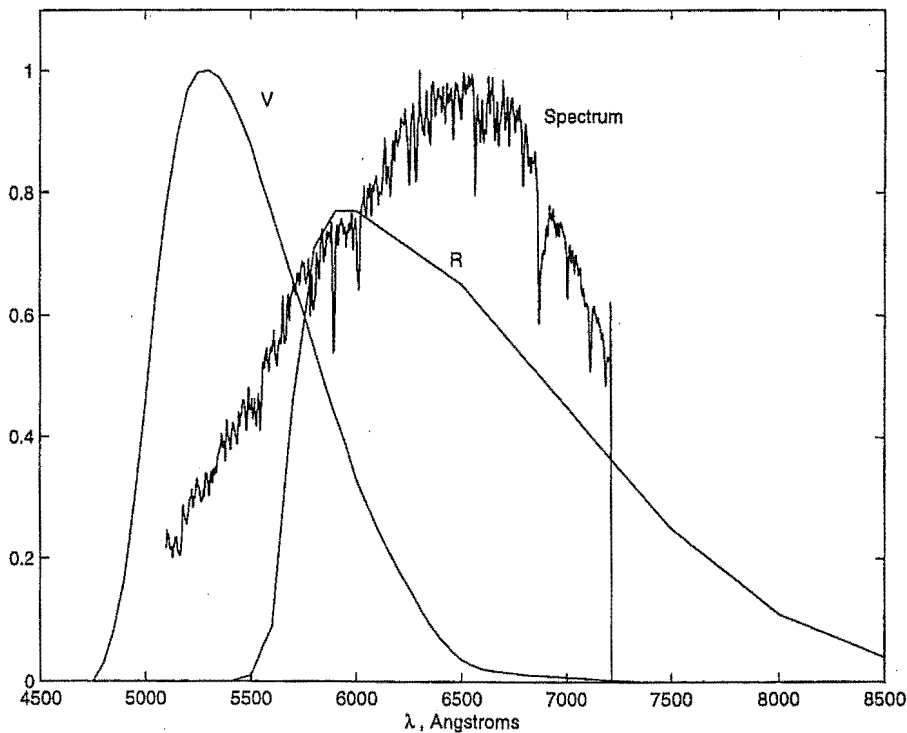
Figure 2.6: A 150 l/mm MRS spectrum, with Cousins V and R filter functions.

If the Cousins filter functions, $V(\lambda)$ and $R(\lambda)$, are multiplied with the raw (non-continuum fitted) spectrum, $S(\lambda)$, and the log of these quantities taken,

then values f_V and f_R are obtained which are proportional to the photometric measurements of V and R, with a factor due to the instrumental response of the spectrograph.

The values $f_V = \int_\lambda S(\lambda)V(\lambda)$ and $f_R = \int_\lambda S(\lambda)R(\lambda)$ were calculated for some RCB stars and 1997 observations of Sakurai's Object for which quasi-simultaneous V and R photometry and MRS spectroscopy were available. A simple rectangular numerical integration over a large number of points was used.

Since the spectra were not taken under photometric conditions these two numbers f_V and f_R are fairly meaningless by themselves. However the quantity

$$m_{s(V-R)} = -2.5 log \frac{f_V}{f_R} \tag{2.1}$$

is proportional to the photometric quantity $(V\text{-}R)$. These values are plotted in figure 2.7. The linear fit appears convincing. The RMS deviation from it is 0.06mag. Using this as a calibration gives a $(V\text{-}R)$ colour for a spectrum taken late in 1996. This is marked on the figure as an asterisk, giving a $(V\text{-}R)$ colour value for a spectrum taken on 1996 September 28 of 0.72.
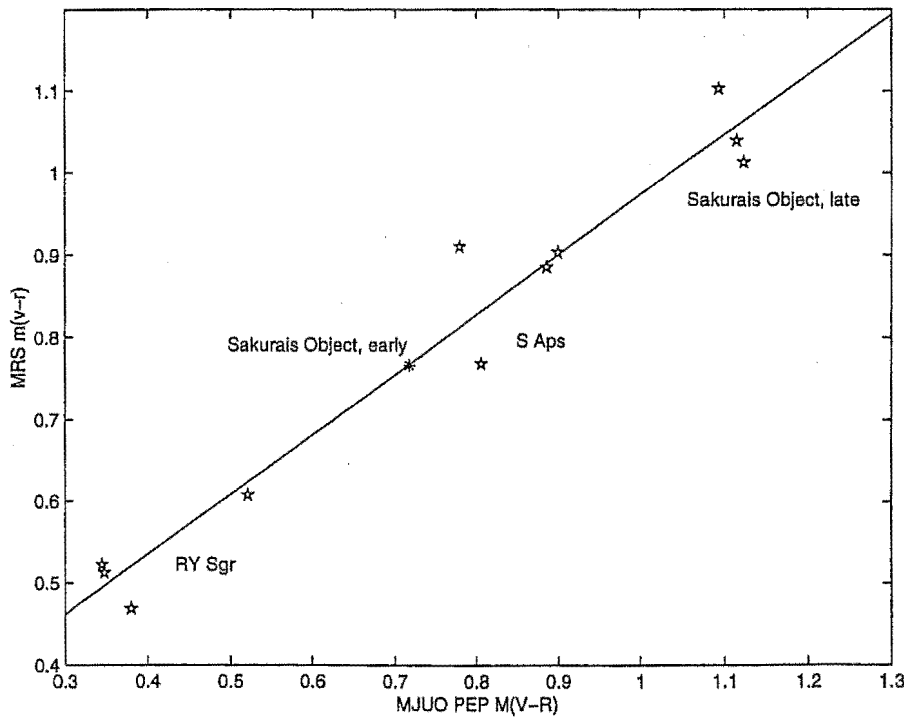
Figure 2.7: A calibration curve using stars of known $(V\text{-}R)$ for which a spectroscopic $(v\text{-}r)$ (MRS m(v-r)) could be calculated. The known $(V\text{-}R)$ colours are from MJUO photoeletric photometry (MJUO PEP). The early Sakurai's Object point for which the $(V\text{-}R)$ colour is required is marked by an asterisk.

This procedure has since become redundant with the publication of 1996 photometry by Duerbeck *et al.* The new photometry does however provide confirmation that the technique is a viable one, as for their last points in 1996, covering the September period the mean *(V-R)* is 0.75.

Chapter 3

Reduction and analysis techniques

3.1 The reduction of MRS spectra of Sakurai's Object

These spectra were reduced using the Figaro package. The reduction procedure follows more or less the procedure devised for the reduction of échelle spectra [10]. Some aspects of the reduction procedure more specific to the spectra of late-type carbon stars are discussed here. A more detailed outline of the general procedure used is in appendix A.

3.2 Continuum fitting

Sakurai's Object is a late-type star with so many absorption lines present that the position of the continuum is difficult to determine. In addition to this, in the period since observations were started at Mt John, molecular bands of various carbon compounds have developed, further distorting the flux distribution of this star. This all makes it very difficult to identify any sort of continuum at all. The continuum would be expected to approximate a blackbody curve dependent on the temperature of the star, with the instrumental profile due to filters, the detector response and the off-blaze-angle response of the grating superimposed. The continuum also falls away at both ends due to instrumental effects such as vignetting within the spectrograph. As the spectrum shows no obvious emission features, there would be no points significantly above the continuum.

An approximation has been made based upon the shape of the flat field lamp spectra (somewhat cooler than Sakurai's Object) and the velocity standard spectra (somewhat hotter than Sakurai's Object and with fewer lines). Lower resolution spectra can also provide some helpful information, as they cover a sufficiently broad region of the spectrum to extend beyond the molecular bands. The Figaro subroutine CFIT allows the user to place points on the spectrum through which a spline is fitted.

To achieve consistency the 150 l mm^{-1} spectra were fitted first, on the assumption that the localised depressions due to bands would have a smaller effect on the overall shape of the spectrum. Figure 3.1 shows one such
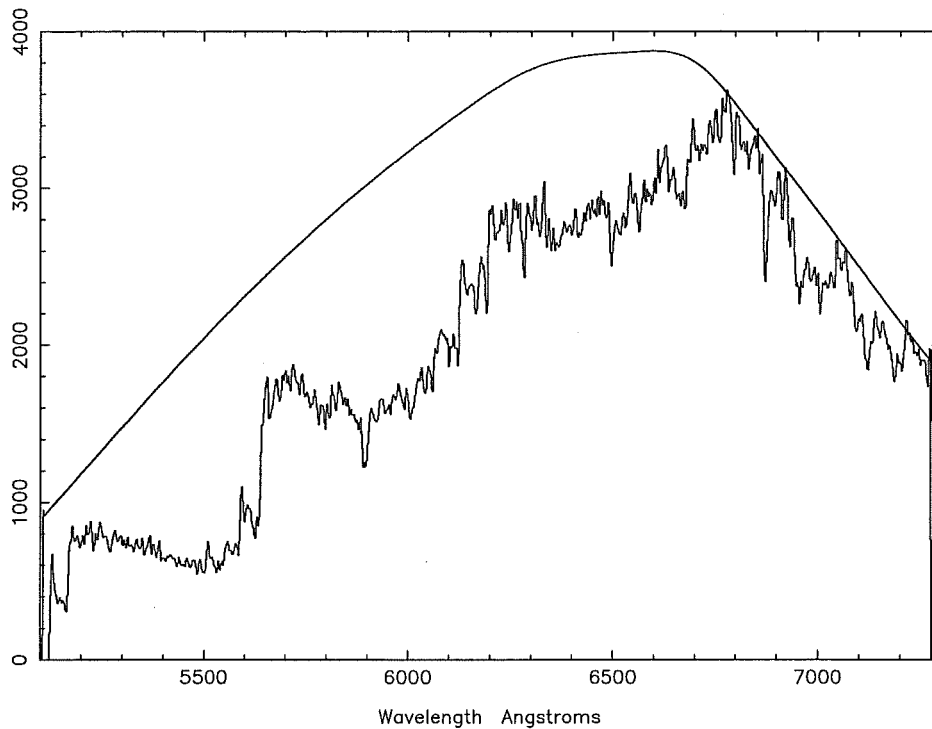
Figure 3.1: An example of a low resolution spectrum (150 l mm^{-1}) with its continuum fit. This spectrum was obtained on 1997 March 12, using the GG475 filter.

150 l mm^{-1} spectrum with a continuum fit. Once this fit was made, higher resolution spectra taken at the same time could be fitted with reference to the low resolution spectra even if the entire wavelength range of the higher resolution spectrum is depressed by molecular bands. A convenient way of doing this is to divide the higher resolution spectrum for which a continuum fit is required, point by point with an already fitted low resolution one. The result is a distribution around the desired continuum fit. This can then be either smoothed, using IXSMOOTH, or be used as a guide when applying CFIT. Usually a combination of both was employed. The process is illustrated in figure 3.2

It should then be possible to compare the depths of molecular bands between low resolution spectra made at different times, and the depths of lines in spectra continuum fitted using the same low resolution spectrum. This can only be done if the depth of the molecular bands has not changed significantly in that time.

To this end, it is useful to have one 150 l mm^{-}1 spectrum for each observing run, preferably with a flat field.
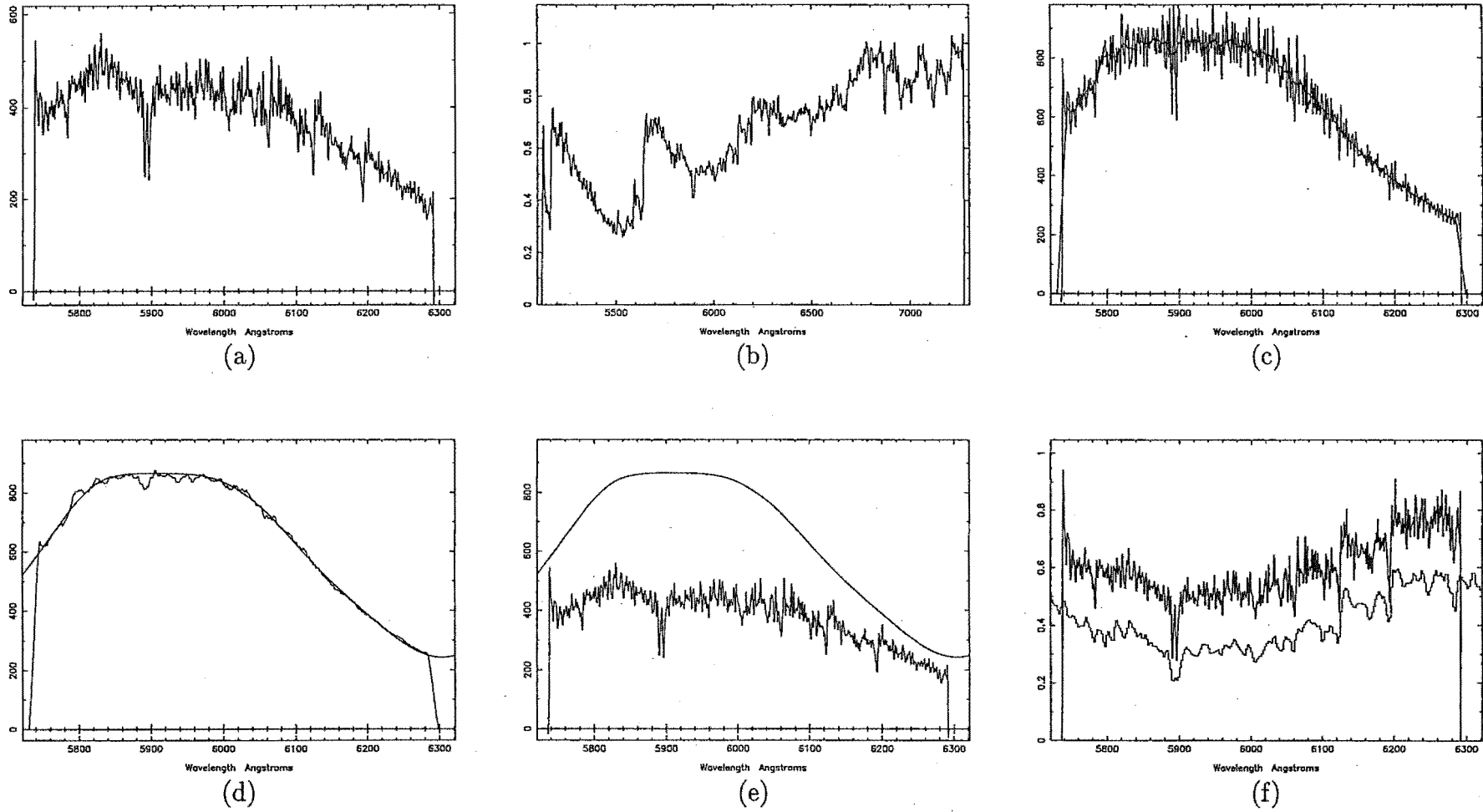
Figure 3.2: The continuum fitting process. The high resolution spectrum (a) is divided by a fully reduced low resolution spectrum

Another way to cope with this problem will be to take spectra of metal deficient stars of similar spectral types, which will hopefully give an almost line-free continuum.

3.3   Line fitting and radial velocities

Spectra obtained using the MRS are obviously not ideal for the determination of very precise radial velocities but reasonable estimates can be obtained from the highest resolution spectra. The Hα and Na D lines have been used in this analysis because they are easily identified in the crowded spectra of Sakurai's Object.

The positions of the Hα and Na D lines were determined by fitting Gaussian profiles to them using the package GAUSS in Figaro. This package allows the user to fit multiple Gaussian profiles to subsets of spectra. The user first defines a continuum or, in the case of Sakurai's Object, a pseudo-continuum by fitting a low order polynomial to selected parts of the spectrum. Then Gaussians are approximately placed on the line or blend to be fitted. The program optimises the fit and returns the central wavelength, width and height of the optimised Gaussian profiles.

GAUSS fits to lines in the helium argon comparison lamp spectra show a maximum uncertainty of about 0.2 Å at the highest resolution, which is equivalent to a Doppler shift of $\pm$ 10 km/s at the position of the Na D lines. Repeated fits with slightly varied initial conditions (eg, continuum position) show an additional uncertainty of $\simeq$ 0.1 Å in using GAUSS to measure the position of a spectral line.

Fits to the Na D lines have proved, if not the most successful, at least the most easily checked for accuracy. In some of the highest resolution spectra four lines are clearly resolved (see figure 3.3). The two larger components are at rest velocity, which in the direction of Sakurai's Object indicates that they are interstellar in origin [1]. In theory, both pairs of lines should have a separation of 5.9 Å. Applying this criterion to fits obtained using GAUSS gives some indication of the quality of these fits. In practice, fits giving separations between 5.7 and 6.1 Å for both pairs of lines were accepted. The resulting fit for April is shown in figure 3.4 and is considered a reasonably good one. The interstellar lines are at 5889.996 Å and 5895.778 Å, separated by 5.78 Å and the stellar ones are at 5891.977 Å and 5898.030 Å, separated by 6.053 Å.

---

[1]Sakurai's Object is located in the direction of the centre of the Galaxy. Looking in this direction interstellar material in orbit around the centre will be moving across the line of sight and therefore have no radial velocity.
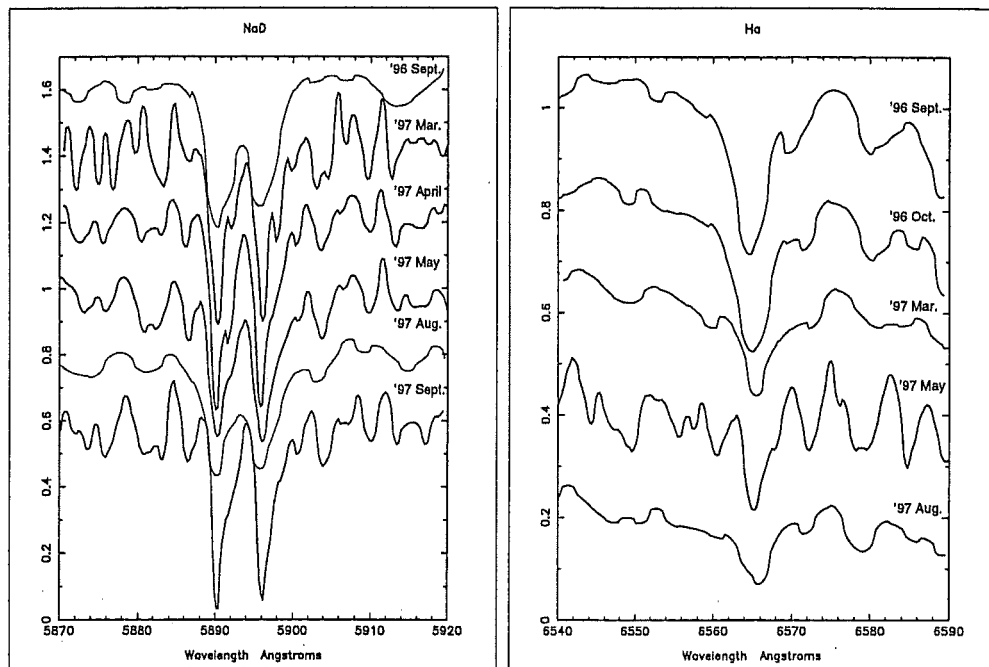
Figure 3.3: Time sequences of the Na D lines Hα lines from MRS spectra. In all of these spectra the local continuum has been normalised to 1 in arbitrary flux units. They have then been offset in steps of 0.2. The Hα lines have been plotted on a larger scale. Thin lines indicate a 300 1 mm^{-1} spectrum while thick ones indicate a 600 1 mm^{-1} spectrum. Differences in the appearance of the later 600 1 mm^{-1} spectra compared to the earliest ones are due to a poorly focussed spectrograph.

The best fits to the Na D and Hα lines show radial velocities of between 86 and 125 km s^{-1} (table 3.1). Within the estimated uncertainties this is in agreement with the radial velocities of 115 km s^{-1} [1] and 125 km s^{-1} [9] obtained by other researchers. These velocities appear to have increased slightly over the period during which these measurements were made. Unfortunately Sakurai's Object is too dim for higher resolution spectroscopy at MJUO using the échelle spectrograph.

date	grating l mm^{-1}	line	meas. λ Å	shift Å	velocity km s^{-1}
1996 Sept 27	300	Hα	6564.746	1.896	86 ± 15
1996 Oct 09	300	Hα	6564.879	2.029	93 ± 15
1997 March 10	300	Hα	6565.368	2.518	115 ± 30
1997 March 14	600	Na D$_1$	5898.003	2.063	104 ± 15
		Na D$_2$	5892.147	2.174	110 ± 15
1997 April 08	600	Na D$_1$	5898.030	2.090	106 ± 15
		Na D$_2$	5891.977	2.004	102 ± 15
1997 May 02	600	Hα	6565.192	2.342	107 ± 15
1997 May 03	600	Na D$_1$	5898.307	2.387	120 ± 15
		Na D$_2$	5892.226	2.253	114 ± 15
1997 Aug 03	300	Hα	6565.375	2.529	116 ± 30
1997 Sept 14	600	Na D$_1$	5892.324	2.351	120 ± 20
		Na D$_2$	5898.402	2.462	125 ± 20

Table 3.1: Measurements of the radial velocity of Sakurai's Object from MRS spectra.
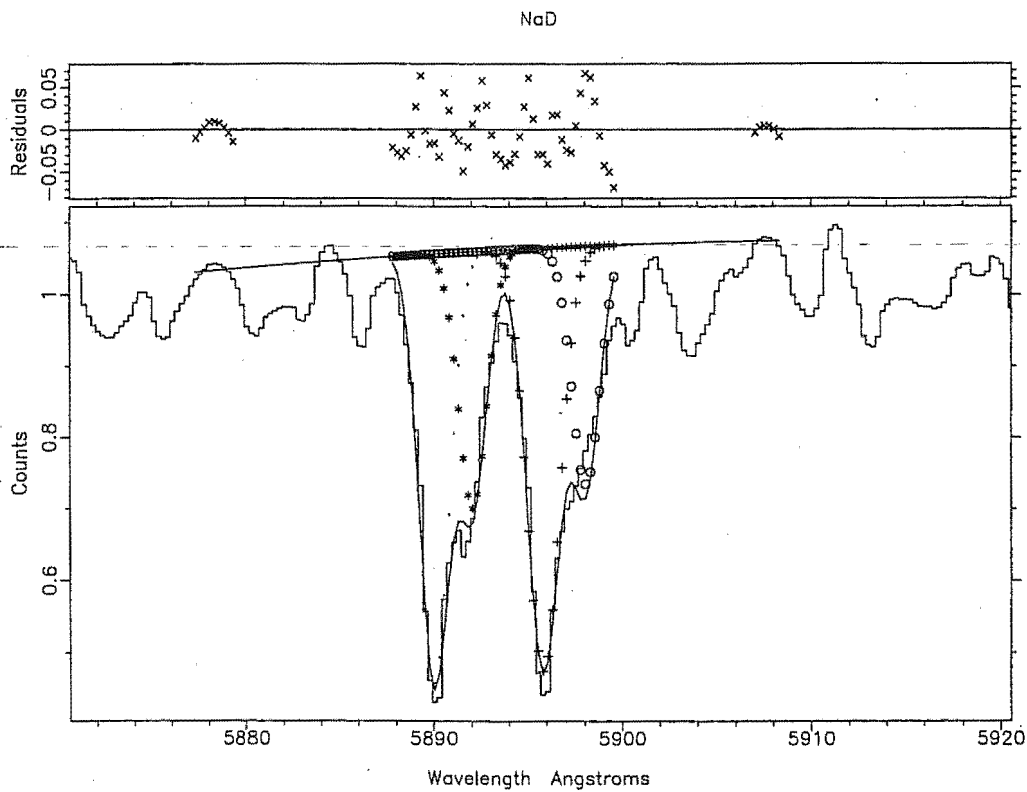
Figure 3.4: A moderately good fit to the Na D lines in a high resolution MRS spectrum. Four Gaussian curves have been used to model these lines from 1997 April.

3.4 Period analysis

Both the MJUO data and the photometric data published by Duerbeck *et al* for 1997 have been analysed for periodicities of less than 100 days. This analysis was done using the Fourier transform code T7, which uses a Lomb-Scargle algorithm. This algorithm is widely used in astronomical work as it deals with data on a point by point basis, and so does not require that the data be evenly spaced in time as Fast Fourier transform algorithms do. The original code for T7 was published by Press and Teukolsky [11] and has since been developed in the Astronomy Research Group at the University of Canterbury by a number of researchers.

Before the data from Duerbeck *et al* could be analysed in this way it was necessary to remove the increasing trend of the data as the star became brighter. This was done by subtracting a linear fit from the data. The unsmoothed data, and the fit used, are plotted in the top panel of figure 3.5 and the smoothed data that was finally used is in the bottom panel. It was not necessary to smooth the MJUO data in a similar fashion because there was no trend in that data set.

The results from this period analysis are presented in chapter 4.
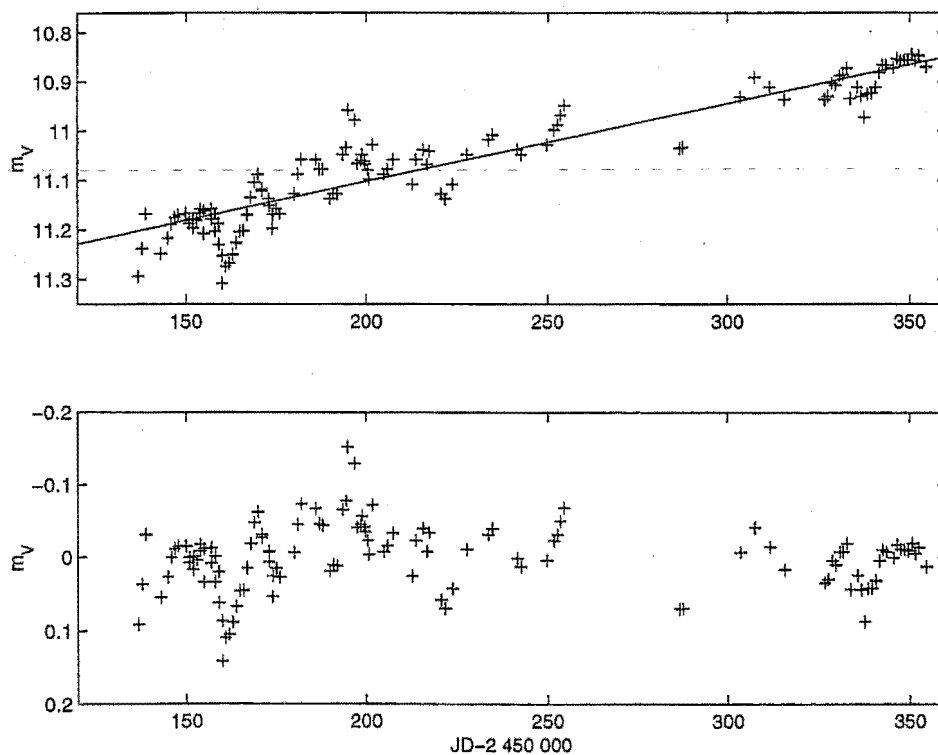
Figure 3.5: Photometric data from Duerbeck et al [9]. Top: before smoothing showing the linear fit to the data, Bottom: after smoothing.

Chapter 4

The physical characteristics of Sakurai's Object

4.1 Spectral classification

The spectral classification of a star is usually defined using the blue end of the visible spectrum between about 3700 Å and 5000 Å. This is due to the historical reason that the standard photographic plates used for spectroscopy were insensitive in the red. Ratios of line strengths are used to define where the star falls in a temperature/luminosity sequence. Late-type carbon stars have had to be classified according to different criteria than the far more common late-type oxygen-rich stars (K and M type). This is mainly due to the presence of the strong bands of carbon compounds, especially in the blue/violet part of the spectrum.

The process of spectral classification is considered to be a preliminary phase in the modelling of the physical processes involved, and is done in such a way as to hopefully avoid any preconceptions about the physical characteristics (eg. temperature) of the stars involved. Keenan [12] has made a revision to the MK system of spectral classifications, which has three sequences of carbon stars, corresponding to three populations, the C-R, C-N and C-H types. These populations have different characteristics such as temperature, velocity and space distribution, and composition. The R and N subtypes were once thought to be of different temperatures but it has since been discovered that the lack of light at the blue end of the spectrum in N type carbon stars is due more to composition than to temperature. C-H stars have strong CH bands present in their spectra. (For further information about the spectral classification of C stars, see Keenan [12].) A spectral atlas of C stars has also been compiled by Barnbaum et al [13] using these new criteria and the spectra presented in this atlas are available in digital form from the Astronomy Data Center (ADC)[1]. The classification sequence is based on C stars, with normal H abundances, whereas Sakurai's Object has been found to be hydrogen deficient [14].

MRS spectra are extremely well suited to spectral classification as they

---

[1]http://adc.gsfc.nasa.gov/

cover wide wavelength regions. From simply overplotting the most likely loo-
king spectra obtained from the ADC with spectra of Sakurai's Object, a near
match could be found.

The spectrum of Sakurai's Object is most like that of HD 223392, which is
assigned a spectral type of C-R3 $C_2$4 CH3.5 in the Barnbaum spectral atlas (see
Figure 4.1), although Sakurai's Object has more depression in the molecular
bands. It is not any earlier in the sequence (hotter) due to the strengths of the
carbon bands, or any later (cooler) due to the fact that there is still some light
present in the blue end of the spectrum. That there is still blue light present
also excludes C-N type stars.

The blue end of the spectrum of HD 223392 is more depressed than that
of Sakurai's Object and does not have the sharply defined C_2 bands. This is
because HD 223392 is not hydrogen deficient and in this section of the spectrum
CH bands, including the G-band, overlap with the C_2 and CN bands creating
the different absorption below 4200 Å.

Sakurai's Object is from the above sequencing a C-R3 $C_2$5 supergiant star,
roughly equivalent to a K2 I star in temperature [12].
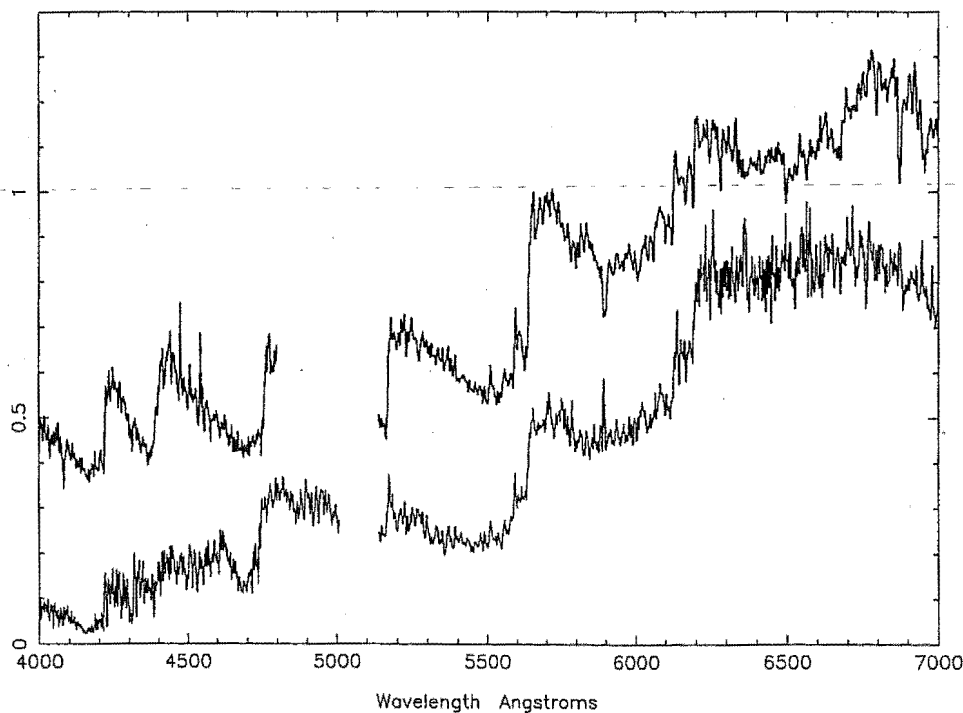
Figure 4.1: A spectrum of Sakurai's Object (above) compared with that of the
carbon star HD223392 (below). Note the difference in absorption below 4700 Å.

A spectrum of V605 Aquilae obtained in 1921 is shown in figure 4.2 and it also has the molecular bands of carbon compounds seen in the spectrum of Sakurai's Object.
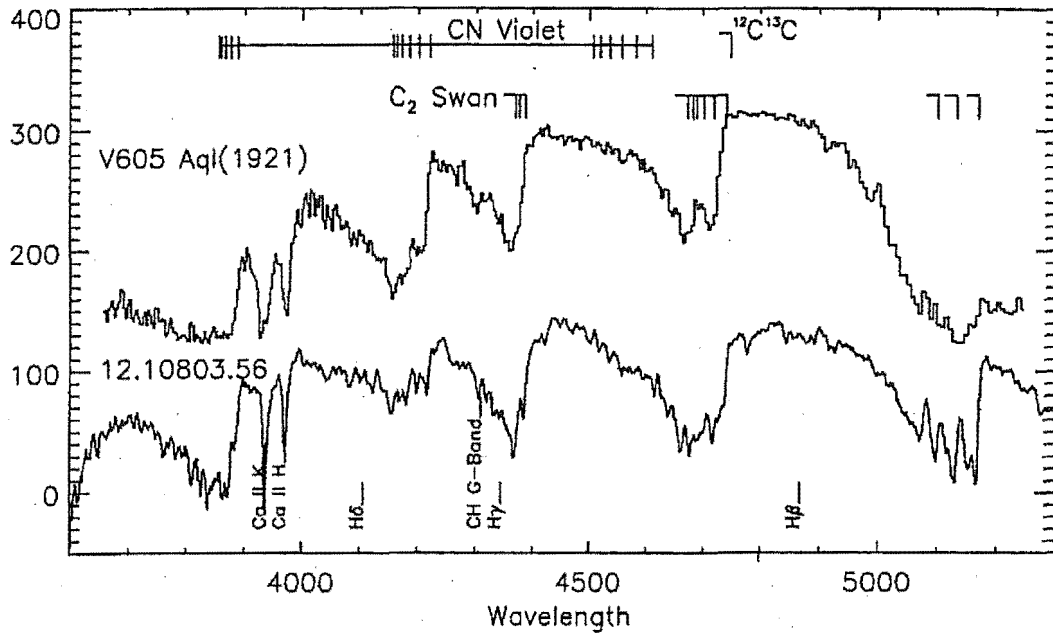
Figure 4.2: The spectrum of V605 Aquilae observed in 1921 . This spectrum shows many of the same features visible in the spectra of Sakurai's Object (Figure 4.1). The lower spectrum is that of MACHO*05:46:46.2-70:38:12.79, an RCB star in the LMC. (Figure from Clayton [5].)

4.2 Determination of bolometric magnitudes

The bolometric magnitude is the magnitude of a star integrated over all wavelengths. Multicolour photometry measures the magnitude of the star in a number of different wavelength regions (passbands). The temperature of the star may be estimated from the ratio of the star's energy in any two passbands. This ratio is expressed as the difference of two magnitudes and is referred to as a colour index, or colour.

A bolometric correction, dependent on that colour index, may be applied to measurements in any one passband to determine the bolometric magnitude of the star. However, before the bolometric correction can be calculated, the photometric data must be corrected for the effects of interstellar extinction. Duerbeck and Bennetti [1] use a value of $E_{B-V} = 0.53$, which was obtained from stellar colours, extinction maps, and the Balmer decrement of the planetary nebula surrounding Sakurai's Object. This was further confirmed by Duerbeck et al [9] by matching reddened synthetic colours to the observed

photometry. Kimeswenger and Kerber [15] use $E_{B-V} = 0.54$, but give no explanation of how that value was obtained.

Given E_{B-V} it is possible to calculate extinctions for the other passbands, for instance the extinction in the Cousins V passband is given by $A_V = R_V E_{B-V}$. The only problem is to obtain a suitable constant,(R_V), which is dependent on the passband itself and the nature of the interstellar absorbing matter.

Two ways of finding the bolometric correction have been used, one which uses the $(B-V)$ colour index to give a correction based on the colours of normal (not hydrogen deficient) stars, and another which uses the $(R-I)$ colour index to give a correction based on carbon stars in the Large Magellanic Cloud.

This means that corrections for the V, R and I passbands were required. Both Astrophysical Quantities [16] and Landolt and Bornstein[17] have similar tables of wavelength versus extinction. The most widely accepted value for R_V is 3.10 ± 0.15 .

The response of the system used at MJUO is not entirely standard, especially in the R and I passbands as a S20 photomultiplier tube is used instead of the gallium arsenide tube prescribed in the Cousins $UBVRI$ filter system (see Bessell [7]). The photomultiplier tube used has a wavelength cutoff in the I filter which effectively moves the peak of that filter function toward the blue. The peaks of the filter functions for the R and I filters at MJUO are $R = 0.575\mu$ and $I = 0.750\mu$. Using these wavelengths to find the extinctions from the tabulated values in Astrophysical Quantities, $\frac{A_R}{A_V} = 0.93$ and $\frac{A_I}{A_V} = 0.68$.

Most of the variables used in this analysis are not well defined. The peak of the flux through any filter is dependent on the colour of the star, and will therefore probably have a different wavelength to the one tabulated.

First, using the *(B-V)* data and the bolometric corrections given for normal supergiant stars in Astrophysical Quantities, M_{bol} was calculated for each individual data point and for the average data points used by Duerbeck *et al*[2].

The bolometric correction was chosen by spline interpolation of the values given in Astrophysical Quantities [16], according to the *(B-V)* colour of the star. It should be remembered that these figures are for late type normal stars, presumably with oxide bands rather than carbon bands.

The second technique is a bolometric correction based on results from Costa & Frogel [18], a study of 888 carbon stars in the LMC. This paper presents *RI* and *JKH* photometry, and gives the following formula utilising *(R-I)* to

---

[2]In their analysis, Duerbeck *et al* used the average of measurements taken over a period of time, in order to negate the effect of any pulsations.

calculate m_{bol}.

$$I_0 - m_{bol} = 1.33(\pm 0.13) \times (R - I)_0 - 1.24(\pm 0.14) \qquad (4.1)$$

Figure 4.3 shows the results of both methods, which are tabulated in table 4.2. There is an RMS difference between the two sets of 0.5 mag. The predicted uncertainty from Costa and Frogel [18] in equation 4.1 is ± 0.34, while using a value of $R_V = 3.10$. The results of calculating the same magnitudes used by Duerbeck et al are also given. These compare well with the results from using the normal supergiant bolometric corrections.
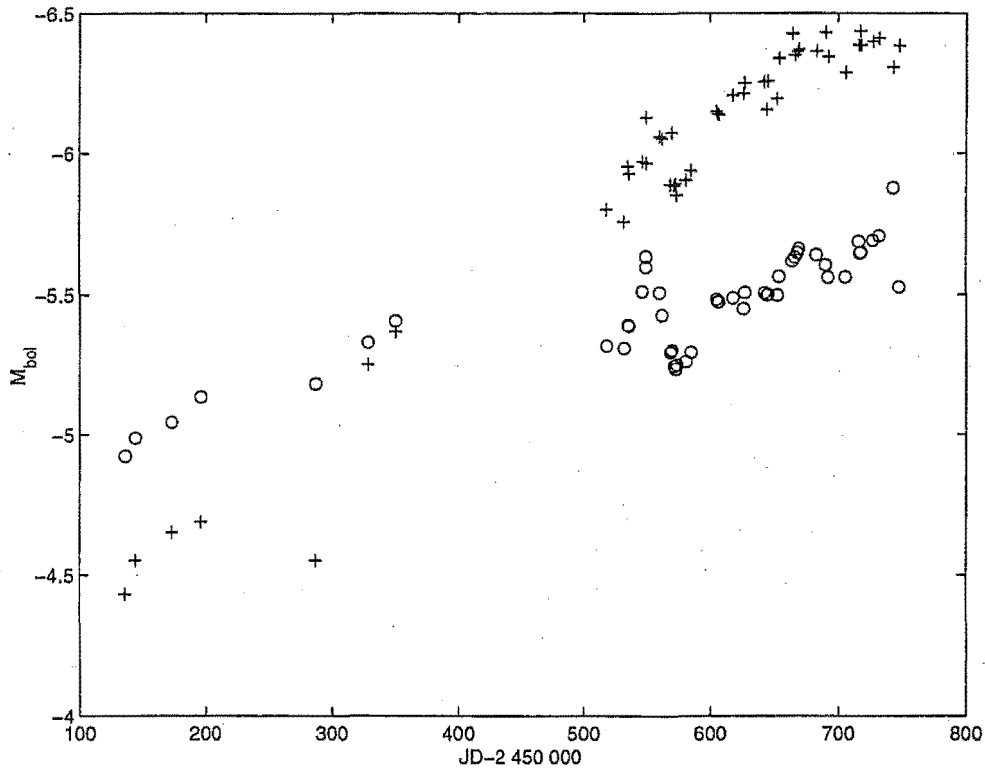
Figure 4.3: The results of the two different bolometric corrections (B.C.) showing the change in absolute bolometric magnitude with time. B.C. using normal supergiant colours are marked with o, those using Costa and Frogel's result are marked with +

The difference between these two sets of results is sensitive to the parameters chosen. If a standard value of $R_V = 3.10$ is used, the mean difference between the two bolometric corrections is 0.56 mag. If the value of R_V is increased to 4.2 this value reduces to $\simeq 0$, although the trend remains. This is also equivalent to altering the value of E_{B-V} by the same proportion since the selective extinction in the different passbands is determined using these numbers.

The fact that the MJUO photometric system is not standard, especially with regard to the I passband may have affected the result. As each obser-

JD-2 450 000	carbon	normal	JD-2 450 000	carbon	normal
136.0000	-4.4	-4.9	607.0306	-6.1	-5.5
144.0000	-4.6	-5.0	618.0407	-6.2	-5.5
173.0000	-4.7	-5.0	625.9945	-6.2	-5.4
196.0000	-4.7	-5.1	626.9468	-6.2	-5.5
287.0000	-4.6	-5.1	642.0406	-6.3	-5.5
328.0000	-5.3	-5.3	643.9843	-6.2	-5.5
350.0000	-5.4	-5.4	645.0583	-6.3	-5.5
518.1827	-5.8	-5.3	652.1641	-6.2	-5.5
532.1974	-5.8	-5.3	653.8762	-6.3	-5.6
535.1735	-6.0	-5.4	663.8594	-6.4	-5.6
536.1766	-5.9	-5.4	665.9308	-6.3	-5.6
547.1082	-6.0	-5.5	668.0400	-6.4	-5.6
550.0000	-6.1	-5.6	668.9736	-6.4	-5.7
550.1357	-6.0	-5.6	682.9663	-6.4	-5.6
560.2496	-6.1	-5.5	689.8946	-6.4	-5.6
562.2373	-6.1	-5.4	691.9590	-6.3	-5.6
569.0521	-5.9	-5.3	705.9713	-6.3	-5.6
570.0641	-6.1	-5.3	715.9511	-6.4	-5.7
572.1222	-5.9	-5.2	716.9062	-6.4	-5.6
573.1402	-5.9	-5.2	717.9030	-6.4	-5.6
573.9932	-5.9	-5.2	726.9002	-6.4	-5.7
581.2312	-5.9	-5.3	731.9098	-6.4	-5.7
585.1160	-5.9	-5.3	742.8572	-6.3	-5.9
605.0308	-6.1	-5.5	747.8815	-6.4	-5.5
606.0483	-6.1	-5.5			

Table 4.1: Absolute bolometric magnitudes calculated from the photometric data using the normal supergiant and the carbon star bolometric corrections, both for a distance of 8kpc.

vation is determined differentially with respect to standard stars, this will be a problem if the energy distributions are different between the standard and the observed stars. This is almost certainly the case. The magnitude of the problem is difficult to estimate, given the unusual colour of Sakurai's Object and the fact that no other differential I magnitudes have been published.

Duerbeck *et al* used the Bessell *UBVR* and Gunn i which means that their i photometry data is incompatible with the bolometric correction from Costa and Frogel. As these data were acquired in 1996 while the star was relatively hot and before it developed the molecular bands in its spectrum, the bolometric correction for normal supergiant stars is probably the best approximation available.

In section 4.8 where these results have been compared to the available models, the data from Duerbeck *et al* [9] have been corrected using the normal supergiant bolometric correction, while for the MJUO photometry form 1997 after the molecular bands formed the bolometric corrections for C stars from Costa and Frogel [18] have been used.

4.3 The distance to Sakurai's Object and the size of its planetary nebula.

There have been three estimates of the distance to Sakurai's Object. The first was made by Duerbeck and Bennetti [1]. A statistical distance of 5.5 kpc was found from the $H\beta$ flux of the surrounding planetary nebula.

Duerbeck *et al* [9] make a second distance estimate based on the observed line of sight velocity of Sakurai's Object (100km s^{-1}) , which along with its galactic co-ordinates, places it near the centre of the Galaxy, based on the work of Pottasch [19] on the distribution of planetary nebulae . The galactic centre is assumed to be 8 kpc away and the same distance is assumed for Sakurai's Object.

The third distance estimate, presented by Kimeswenger and Kerber [15] is 1.1 kpc. This method uses the amount of interstellar reddening, and is calibrated by making estimates of the absolute magnitude, the distance to and the amount of reddening towards the stars in the direction of Sakurai's Object.

These last two distances place Sakurai's Object in two very different parts of the Galaxy. With its galactic coordinates of $l = 10°.48$, $b = 4°.41$ the first distance of 8 kpc places the object in the galactic bulge, some 600 pc from the plane of the Galaxy, while 1.1 kpc places it in the neighbourhood of the Sun, 80pc from the plane (Figure 4.4). Neither of these positions are unusual places for a PN to be found.
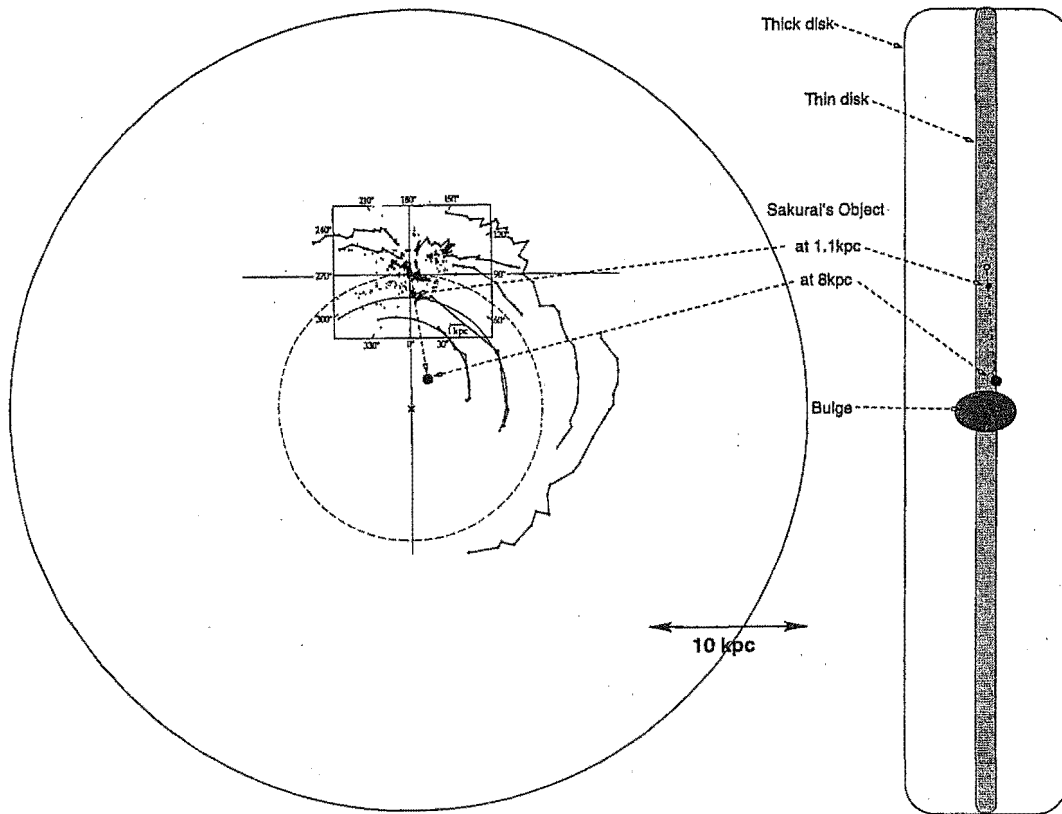
Figure 4.4: Two possible positions of Sakurai's Object in the Galaxy are shown, a small filled circle at 1.1 kpc and a large filled circle at 8 kpc. The Sun is marked as an open circle. The dark lines in the plan view mark the positions of the spiral arms as indicated by 21cm observations of neutral hydrogen[20].

The angular diameter of the surrounding PN is 32" giving a diameter of 0.17 pc at a distance of 1.1 kpc or 1.2 pc at a distance of 8 kpc. Kimeswenger and Kerber state that the smaller radius, and therefore their distance, is more compatible with the central star being highly luminous. This argument is invalid if the central star is "born again" and the PN was ejected at a much earlier luminous stage. The other final flash candidates, A30 and A78 have diameters of 0.53 and 0.45 pc respectively, V605 Aql (A58), 0.62pc and FG Sge, 0.39pc [1].

An accurate distance to Sakurai's Object is vital for any meaningful comparison of observation with theory. The independent estimates of the distance to Sakurai's Object do not overlap and there are valid arguments for and against both extremes. Both extremes of distances have been used in the subsequent calculations, and their consequences with respect to currently available astrophysical models are discussed later.

4.4 The temperature of Sakurai's Object

Sakurai's Object is in the process of expanding and cooling. Duerbeck *et al* have derived temperatures by comparing the (*B-V*) colour observed throughout 1996 to synthetic colours from model atmospheres of hydrogen-deficient carbon stars computed by Asplund *et al* [14].

For their photometric observations in early 1997 Duerbeck *et al* [9] give a temperature of 6000 K. Their (*B-V*) values for early 1997 agree moderately well with the values from MJUO, bearing in mind that each of their points are the mean of a small number of observations. Unfortunately the three measurements taken in 1997 are clustered around a localised maximum in the light curve and are therefore not entirely representative of the time period (see figure 2.4).

Using Asplund *et al*'s synthetic colours for C star model atmospheres these values indicate that Sakurai's Object has cooled from 6000 K to somewhere around about 5000 K. Asplund's models only go down to 5000 K but he notes in the text that the predictions tend to be 500 K hotter than the spectroscopic evidence from real RCB stars would suggest. This is attributed to the models having too high a metallicity.

Using Duerbeck *et al*'s colours and Asplund *et al*'s model colour/temperature estimates for the RCB stars, the temperatures found are about 100 degrees higher than those reported by Duerbeck.

In a private communication Asplund has expressed some misgivings about using his colours in this way, as the composition of Sakurai's Object differs from that used in the models. The models have a C/He ratio of 1% whereas Sakurai's Object has a C/He of approximately 10%. This means that for a given temperature, Asplund's models will be redder than Sakurai's Object, so temperatures estimated from those models will tend to be too high. The model temperatures, less 500 K, have been used as an upper limit for the temperature of Sakurai's Object. New estimates will have to be made as better models become available.

4.5 The radius of Sakurai's Object

The radius of the star can be calculated using the following relationship.

$$\frac{L}{L_\odot} = (\frac{R}{R_\odot})^2(\frac{T}{T_\odot})^4 \qquad (4.2)$$

or

$$\log(\frac{R}{R_\odot}) = \frac{1}{2}\log\frac{L}{L_\odot} - 2\log\frac{T}{T_\odot} \qquad (4.3)$$

For the period covered by the MJUO observations, during which the radius appears to have increased linearly, this yields an average expansion of $0.3R_\odot$ day^{-1} during 1997, which is higher than that reported by Duerbeck et al for 1996, but consistent with their observation that the rate of expansion appears to be increasing. Figure 4.5 shows the calculated radius as a function of time.

The surface of Sakurai's Object is therefore moving at 2.6 kms^{-1}, equivalent to a Doppler shift of 0.04Å relative to the rest velocity of the system, defined by the velocity of the nebula.

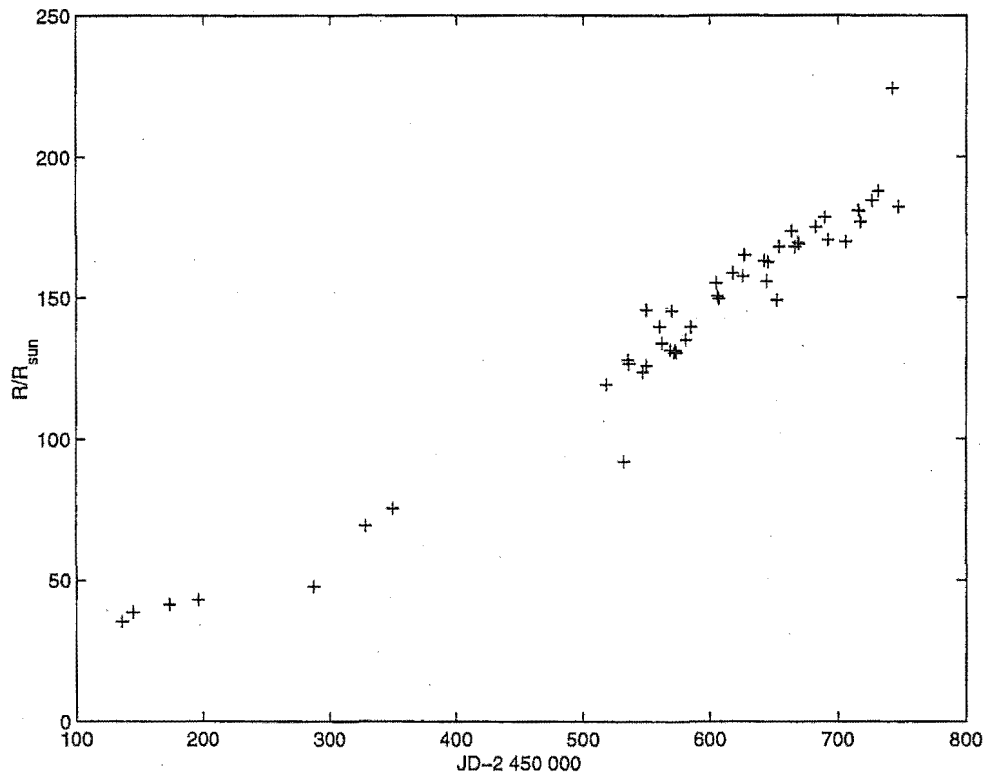Figure 4.5: The radius of Sakurai's Object as a function of time, calculated for a distance of 8kpc.

4.6 Results

Table 4.2 presents the physical parameters calculated for Sakurai's Object from the photometric data obtained from MJUO. The bolometric corrections used to correct these results come from the equation given by Costa and Frogel [18]. The absolute bolometric magnitudes, and hence the luminosities and radii that

have been calculated from them, using both 8kpc and 1.1kpc as the distance measurement.

Also included at the top of the table are the eight data points used by Duerbeck *et al* [9] in their photometric analysis of Sakurai's Object. Each of these eight points is the average of a number of observations over a short period of time. For these points the bolometric correction for normal supergiant stars has been tabulated and the subsequent properties derived from that.

These results show a decrease in temperature and an increase in luminosity and radius during 1996 and 1997. The luminosity has continued to increase although the V magnitude peaked at some time during the seasonal break. The significance of these results with respect to the models of final flash objects is discussed in section 4.8

4.7   Short term variability

In addition to the overall increase in luminosity observed in Sakurai's Object, there are variations in brightness on timescales shorter than 100 days.

Photometry from JD 2 450 136 to JD 2 450 556 has been published by Duerbeck *et al* [9]. Photometry also has been obtained at MJUO from JD 2 450 505 to JD 2 450 747. Both data sets are shown in figure 2.4.

Duerbeck *et al* find evidence for periodicities of 63, 25, 14 and 8 days through Fourier analysis. By a different method applied to the residuals from the 63-day curve, they find periods of 22.0, 13.8 and 7.7 days.

Multiple attempts at fitting the same data sets used by Duerbeck *et al*, using the Lomb-Scargle Fourier analysis program T7 (see section 3.4) indicate a period of between 58 and 72 days, and others of about 21, 13 and 7 days.

In the MJUO data set, a period of 60 days and an amplitude of 0.1 mag was found using this Fourier Transform technique. No other periods could be reliably identified. This may be because the data sampling is sparse or possibly because, as the star becomes cooler, some modes are no longer unstable to pulsation. This is illustrated in figures 7 and 8 of Duerbeck *et al* [9]. The most obvious thing about the light curve of Sakurai's Object during 1997 is that it varies over a much larger range, ~ 0.5 magnitudes, compared to ~ 0.1 in 1996.

Figure 4.6 shows the data from Duerbeck *et al* with a synthetic curve compounded from periods of 58 and 21 days. These data have had an overall increasing trend removed (see section 3.4). The MJUO data, is shown in the lower panel with a synthetic curve of 60 days.

JD-2 450 000	m_v	Temp (K)	B.C.	M_{bol}	$\log L/L_\odot$ 8kpc	$\log R/R_\odot$	M_{bol}	$\log L/L_\odot$ 1.1kpc	$\log R/R_\odot$
136.0	11.29	7550	-0.05	-4.9	3.8	1.6	-0.6	2.1	0.8
144.0	11.21	7400	-0.04	-4.9	3.8	1.7	-0.6	2.1	0.8
173.0	11.15	7350	-0.04	-5.0	3.9	1.7	-0.7	2.1	0.8
196.0	11.05	7250	-0.03	-5.1	3.9	1.7	-0.8	2.2	0.9
287.0	11.03	6700	-0.05	-5.1	3.9	1.8	-0.8	2.2	0.9
328.0	10.91	6500	-0.08	-5.3	4.0	1.8	-1.0	2.2	1.0
350.0	10.85	6400	-0.10	-5.4	4.0	1.9	-1.0	2.3	1.0
550.0	10.87	5500	-0.30	-5.3	4.0	2.0	-1.0	2.2	1.1
518.2	11.14	5650	-0.61	-5.8	4.2	2.1	-1.4	2.4	1.2
532.2	10.97	6350	-0.68	-5.7	4.1	2.0	-1.4	2.4	1.1
535.2	11.07	5650	-0.56	-5.9	4.2	2.1	-1.6	2.5	1.2
536.2	11.07	5600	-0.58	-5.9	4.2	2.1	-1.6	2.5	1.2
547.1	10.91	5750	-0.65	-5.9	4.2	2.1	-1.6	2.5	1.2
550.1	10.84	5700	-0.66	-5.9	4.2	2.1	-1.6	2.5	1.2
560.2	10.99	5500	-0.56	-6.0	4.3	2.1	-1.7	2.5	1.3
562.2	11.03	5650	-0.54	-6.0	4.3	2.1	-1.7	2.5	1.3
569.0	11.22	5450	-0.54	-5.8	4.2	2.1	-1.5	2.5	1.2
570.0	11.23	5450	-0.43	-6.0	4.3	2.2	-1.7	2.5	1.3
572.1	11.27	5500	-0.51	-5.8	4.2	2.1	-1.5	2.5	1.2
573.1	11.28	5500	-0.50	-5.8	4.2	2.1	-1.5	2.5	1.2
573.9	11.28	5450	-0.53	-5.8	4.2	2.1	-1.5	2.5	1.2
581.2	11.28	5400	-0.50	-5.9	4.2	2.1	-1.5	2.5	1.3
585.1	11.26	5350	-0.49	-5.9	4.2	2.1	-1.6	2.5	1.3
605.0	11.09	5350	-0.48	-6.1	4.3	2.2	-1.8	2.6	1.3
606.0	11.06	5400	-0.50	-6.1	4.3	2.2	-1.8	2.6	1.3
607.0	11.06	5450	-0.51	-6.1	4.3	2.2	-1.8	2.6	1.3
618.0	11.08	5350	-0.46	-6.2	4.3	2.2	-1.8	2.6	1.3
625.9	11.10	5400	-0.44	-6.2	4.3	2.2	-1.9	2.6	1.3
626.9	11.08	5300	-0.43	-6.2	4.3	2.2	-1.9	2.6	1.3
642.0	11.06	5350	-0.43	-6.2	4.3	2.2	-1.9	2.6	1.3
643.9	11.07	5350	-0.49	-6.1	4.3	2.2	-1.8	2.6	1.3
645.0	11.06	5350	-0.44	-6.2	4.3	2.2	-1.9	2.6	1.3
652.1	11.00	5500	-0.51	-6.1	4.3	2.2	-1.8	2.6	1.3
653.8	10.99	5350	-0.43	-6.3	4.4	2.2	-2.0	2.7	1.4
663.8	10.93	5400	-0.42	-6.4	4.4	2.2	-2.1	2.7	1.4
665.9	10.92	5400	-0.46	-6.3	4.4	2.2	-2.0	2.7	1.4
668.0	10.91	5350	-0.47	-6.3	4.4	2.2	-2.0	2.7	1.4
668.9	10.89	5400	-0.47	-6.3	4.4	2.2	-2.0	2.7	1.4
682.9	10.95	5300	-0.44	-6.3	4.4	2.2	-2.0	2.7	1.4
689.8	10.97	5300	-0.37	-6.4	4.4	2.2	-2.1	2.7	1.4
691.9	11.01	5350	-0.42	-6.3	4.4	2.2	-2.0	2.7	1.4
705.9	11.04	5300	-0.44	-6.2	4.4	2.2	-1.9	2.6	1.4
715.9	10.98	5250	-0.45	-6.3	4.4	2.2	-2.0	2.7	1.4
716.9	10.95	5300	-0.40	-6.4	4.4	2.2	-2.1	2.7	1.4
717.9	10.94	5300	-0.45	-6.3	4.4	2.2	-2.0	2.7	1.4
726.9	10.94	5200	-0.44	-6.3	4.4	2.3	-2.0	2.7	1.4
731.9	10.94	5150	-0.44	-6.4	4.4	2.3	-2.1	2.7	1.4
742.8	11.04	4600	-0.45	-6.3	4.4	2.3	-1.9	2.6	1.5
747.8	11.10	5200	-0.37	-6.3	4.4	2.3	-2.0	2.7	1.4

Table 4.2: The physical parameters of Sakurai's Object during 1996 and 1997. The first eight points are those used by Duerbeck *et al* the rest are from the MJUO photometry
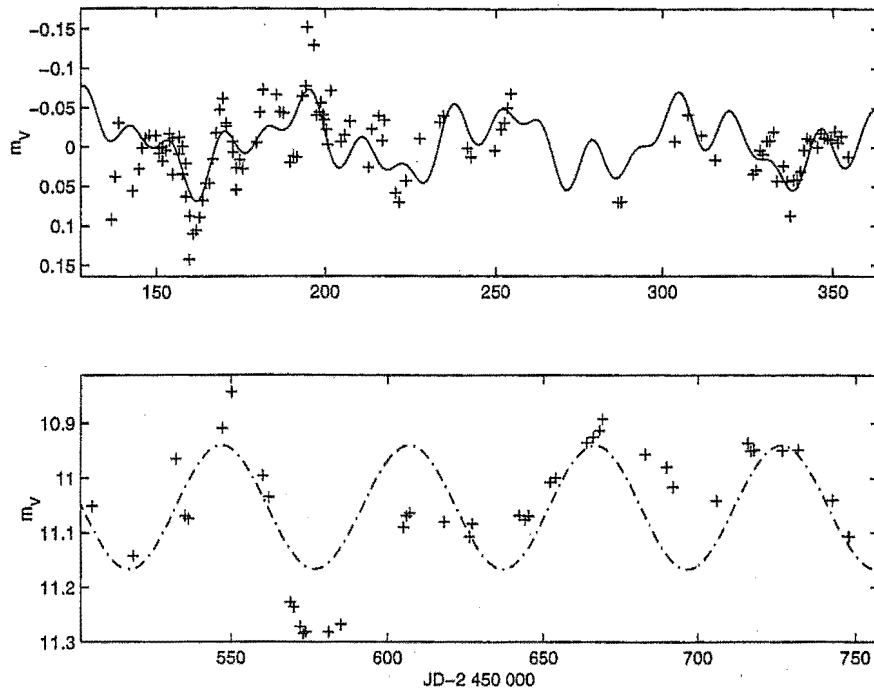
Figure 4.6: Synthetic curves fitted to the short term variations of Sakurai's Object. Top is Duerbeck *et al*'s data with periods of 58 and 21 days fitted, below is MJUO data with a period of 60 days fitted.

4.8 Interpreting the observations as a final flash object

Iben has done a lot of work on the modelling of planetary nebulae and most of the following figures and models are taken from his review paper "Planetary nebulae and their central stars - origin and evolution." [3]. These models show that some planetary nebulae nucleii start burning helium again after they have commenced the white dwarf cooling sequence.

Convection plays an important part in such models, in both bringing processed material to the surface of the star and moving unprocessed hydrogen to depths at which it can undergo fusion. Along with some possible mass loss in the form of a stellar wind, this convective dredging accounts for the unusual surface composition of this type of star. The observed O/C and N/C ratios of Sakurai's Object, calculated from the abundances presented by Kipper and Klochkova [21] are similar to those found in the PNNe A78 and NGC 6751, which are in turn similar to the model abundances for final helium flash stars [3].

An evolutionary track for a $0.6 M_{\odot}$ star after it has left the asymptotic giant branch for the first time is shown in figure 4.7. At t=0 on the dashed line, the star has become hot enough to illuminate the surrounding PN. About 18 600 years after this time, the model undergoes a final helium flash which sends it
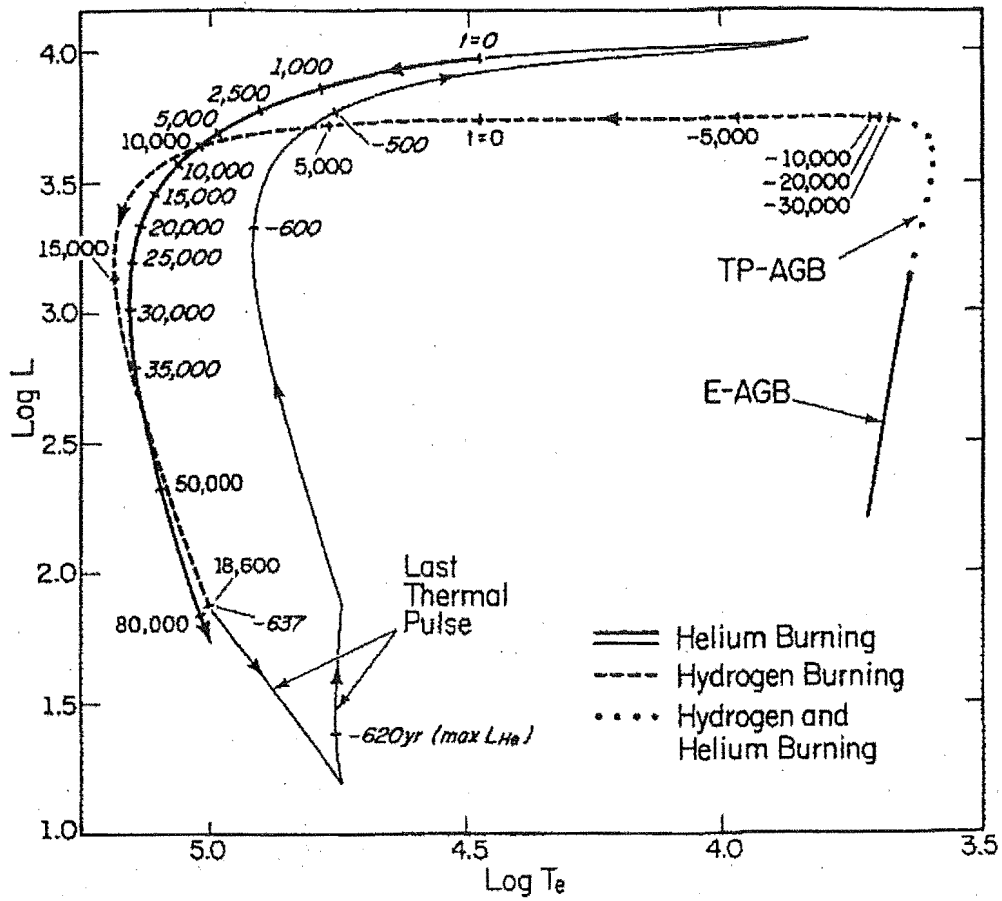
Figure 4.7: The evolutionary track for a $0.6 M_\odot$ final helium flash star [2].
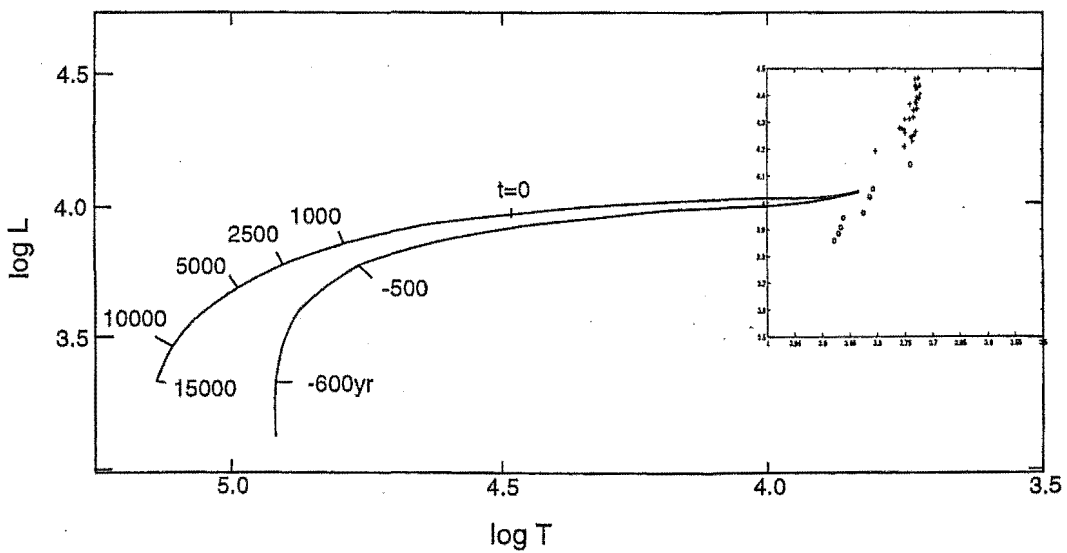

Figure 4.8: The physical parameters of Sakurai's Object superimposed on the evolutionary track in figure 4.7.

back to a position of high luminosity and low temperature. It is believed to be during this rise back to the red giant phase that Sakurai's Object has been discovered and observed.

The physical characteristics derived from the photometric observations of Sakurai's Object, with an assumed distance of 8kpc, have been placed on an enlarged portion of this diagram in figure 4.8. Bearing in mind that the temperatures derived from Asplund's models are an upper limit, Sakurai's Object is seen to be cooler and slightly more luminous than this particular model predicts.

Especially interesting to note is the steep slope around the turnaround point of the evolutionary track. This is not seen in the model, which may not have been calculated on a fine enough time scale to predict such an event. This can also be seen as evidence for the larger distance being more likely, as the luminosities calculated for the shorter distance ($\frac{L}{L_\odot} \simeq 2.5$) are too low to fit any of Iben's models.

Chapter 5

Sakurai's Object in context

5.1 A comparison with other final flash objects

Sakurai's Object can now be placed in context with other suspected final flash objects. These other objects may provide some idea as to what to expect in the future.

5.1.1 The rise ...

Sakurai's Object has continued to increase in brightness since its discovery in early 1996. It has brightened by some 5 magnitudes in V since its discovery. Of the other two possible final flash objects, this time scale is most similar to V605 Aquilae, which increased by 5 magnitudes over a period of about two years. By comparison, the other final flash object, FG Sagittae brightened by ~ 4 magnitudes over a period of seventy years.

5.1.2 ... and fall of Sakurai's Object

As the luminosity of this object continued to increase until the end of the 1997 observing season this subsection may be a little premature. However, in 100% of the cases so far, the carbon rich, hydrogen deficient final flash object has produced an obscuring cloud of carbon dust at some stage in its evolution. V605 Aquilae disappeared from sight some 7 years after its outburst in 1917 due to the formation of a thick cloud of dust. It still remains obscured. FG Sagittae has recently started to show RCB-like declines.

Sakurai's Object may have already started to produce small amounts of dust, causing the short term fluctuations in brightness during 1997. No infrared excess indicative of dust was observed by IRAS in 1983 [1]. It would be interesting to see if there was any infrared excess associated with the object now.

The models predict that a final flash object will increase in temperature at near constant luminosity, over a timescale of ~ 200 years.

5.1.3 The surrounding nebulosity

The planetary nebulae surrounding final flash objects are large, with diameters of about half a parsec. The nebula around Sakurai's Object, if a distance of 8kpc is assumed, has a diameter of 1.2pc, which is twice the size of A58, the nebula around V605 Aquilae. This could indicate that 8kpc is too large a distance. On the other hand, the alternate distance of 1.1kpc gives, along with a much lower luminosity, a PN diameter of 0.17pc less than half the diameter of the PN around FG Sagittae, which would seem to be too small.

Of the four final flash objects, three of them (A30, A78 and V605 Aquilae) have knots of hydrogen deficient nebulosity associated with them. Evidence of such a knot forming around Sakurai's Object should be looked for over the next few decades.

5.1.4 The origin of the R Coronae Borealis stars

The final flash scenario is one of the possibilities suggested for the origin of the dust producing RCB stars. Of the five (including Sakurai's Object) possible FF candidates discussed four have definitely produced dust. Two (FG Sge and V605 Aql) have undergone RCB like decline/recovery phases, although V605 Aql has since disappeared inside a dust cloud. FG Sge has a similar spectral type to other RCB stars. It appears that final flash objects may produce RCB stars, but are more likely to vanish from sight completely in a cloud of dust. Which path Sakurai's Object takes remains to be seen.

5.2 Future observations

Sakurai's Object appears to be evolving on a timescale similar to that of V605 Aquilae, which since its brightening in 1917 has developed molecular bands, ejected a highly opaque dust cloud and more recently evolved toward hotter temperatures ($\sim$50 000 K). From this comparison it can be expected that Sakurai's Object has not yet finished its current stage of rapid morphological change. Ongoing frequent photometric monitoring of Sakurai's Object should therefore be maintained, for three reasons.

The short term variability of Sakurai's Object is not yet well defined and may be evolving as the radius and temperature continue to change. If the variability is the result of pulsations then this star might provide an instructive example of variability at constant mass, but differing luminosities and temperatures.

Dust production similar to that of the RCB stars may happen, or indeed may have already happened in a small way. Both previous final flash objects,

V605 Aql and FG Sge have produced dust. V605 Aql disappeared from sight in 1923 after two RCB-like declines and has remained shrouded in dust ever since. FG Sge, in line with its slower evolution, has only recently (1992) started showing these RCB declines.

When observations ended in 1997 Sakurai's Object was still becoming cooler and brighter. According to the available models, this behaviour will stop and the star will become hotter again, while maintaining a constant luminosity. Determining the rate at which these changes take place can provide some observational constraints on the models and if Sakurai's Object continues to evolve on a similar timescale to V605 Aql these changes can be expected to happen in tens of years rather than tens of thousands of years.

It could also be useful to continue obtaining medium resolution spectra, when practical, perhaps as part of an RCB monitoring program, and also to be able to obtain spectra at short notice if any profound photometric changes are observed.

5.2.1 Dust

Early in 1997 the MJUO photometry shows a relatively large decline in brightness of ~ 0.5 mag. This is much larger than the corresponding variations in Duerbeck's data. Whether this variation is due to some internal change in the pulsational characteristics of the star or the production of dust near the surface is undecided. There may be some possibility of investigating this problem further through the use of two colour or colour-magnitude plots, but this is further complicated by the fact that the star is intrinsically changing in colour. Some estimate of reddening, based on the star only and not that the surrounding nebula and independent of the colour and composition of the star is required. Infrared observation might also show evidence of dust.

5.3 Summary : Sakurai's Object in 1996 and 1997

Sakurai's Object has been observed throughout 1997, and similar observations are available for 1996. During this time it decreased in temperature from 7800K to 5200K, and increased in luminosity by a factor of 4. The temperature became low enough for a significant amount of carbon containing molecules (C_2 and CN) to form. The star's spectral type changed from a G supergiant to a C-R3 supergiant.

If a distance of 8kpc is assumed, its luminosity has increased from $\log\frac{L}{L_\odot} = 3.8$ to 4.4. If the alternate distance of 1.1 kpc is used, then the luminosity has changed from $\log\frac{L}{L_\odot} = 2.1$ to 2.7. The temperature and luminosity calculated

for a distance of 8kpc locate Sakurai's Object at the coolest extent of the final flash evolutionary track for a 0.6 $M_\odot$ planetary nebula nucleus [3]. This is evidence for this object being located closer to 8kpc than 1.1 kpc. However, the relationship between the temperature and luminosity of the object increases rather more steeply than Iben's model would predict.

The change in temperature and luminosity is consistent with the object expanding from $40R_\odot$ to $200R_\odot$. The rate of the expansion appears to have increased over this time, from $\sim 0.1R_\odot\mathrm{day}^{-1}$ to $\sim 0.3R_\odot\mathrm{day}^{-1}$.

At the end of the 1997 observing season Sakurai's Object was still increasing in luminosity. It is expected that eventually this increase will cease and the object will evolve at constant luminosity back to higher temperatures.

5.4   Postscript

Sakurai's Object is fading as predicted. This IAU circular dated 1998 February 19 has recently been received by e-mail from Asplund announcing the first visual decline of Sakurai's Object.

```
1998 February 19              (6824)           Daniel W. E. Gree


                                            Circular No. 6825
Central Bureau for Astronomical Telegrams
INTERNATIONAL ASTRONOMICAL UNION
Mailstop 18, Smithsonian Astrophysical Observatory, Cambridge,
MA 02138, U.S.A.
IAUSUBS@CFA.HARVARD.EDU or FAX 617-495-7231 (subscriptions)
BMARSDEN@CFA.HARVARD.EDU or DGREEN@CFA.HARVARD.EDU (science)
URL http://cfa-www.harvard.edu/iau/cbat.html
Phone 617-495-7244/7440/7444 (for emergency use only)




V4334 SAGITTARII
     W. Liller, Instituto Isaac Newton, Vina del Mar, Chile; M.
Janson, Groningen University; H. W. Duerbeck, Muenster University;
and A. van Genderen, Leiden University, report that this object (cf
IAUC 6718) has faded by almost 2 mag since last November, indicatir
that the predicted dust formation (Duerbeck et al. 1997, A.J. 114,
1657) from the presumed final helium flash has begun.  During 1997
```

Mar.-Nov., the star was between V = 10.75 and 11.0. Subsequent V magnitudes by Liller (L; 0.2-m telescope) and by Janson (J; ESO Dutch 0.9-m telescope): 1997 Nov. 21.02 UT, 10.76 (L); 1998 Feb. 9.37, 11.96 (L); 10.35, 11.90 (L); 14.38, 12.73 (J); 15.38, 12.75 (J); 17.36, 12.74 (J). The star has also become generally redder; between 1997 Sept. 14 and 1998 Feb. 15, U-B changed from +0.83 to +1.12, B-V from +1.66 to +1.51, V-R from +1.11 to +1.71, and V-i (Gunn i) from 2.08 to 2.86. Multicolor optical monitoring is bein carried out, and infrared photometry is encouraged.

Some visual estimates have also been received from Albert Jones and these are plotted with the ESO La Silla V data in the IAU circular and the MJUO data for 1996 in figure 5.1. Ljiljana Skuljan is currently obtaining MRS spectra at MJUO.
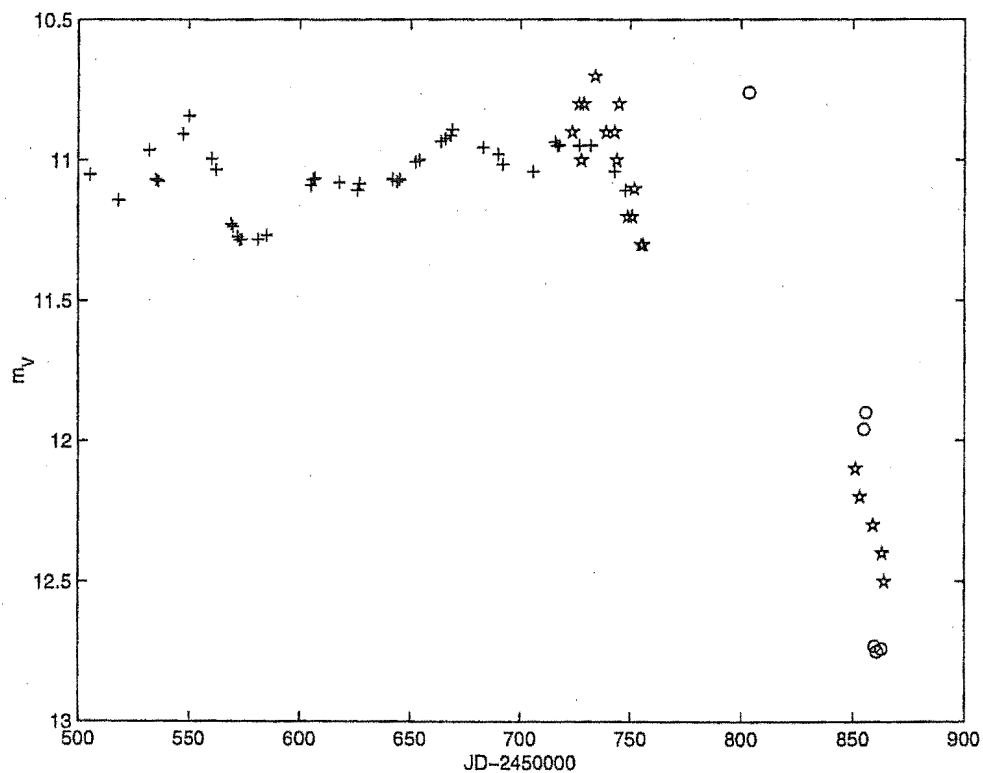

Figure 5.1: Sakurai's object is going into decline. The data from La Silla published in the IAU circular is plotted as ○ and observations made by Albert Jones are marked with ⋆. For comparison the 1996 photometry from MJUO is also plotted.

Chapter 6

Acknowledgements

I would like to thank Peter Cottrell for offering me this project and for his advice and cheerful encouragement throughout the year. I would also like to thank Florian Kerber for bringing this once in a lifetime object to our attention.

This project would not have happened without the help of the technical staff at MJUO, especially Alan Gilmore and Pam Kilmartin who obtained the photometric data used in this study. I would also like to thank Alan and Pam for some excellent dinners and company while I was observing at Mount John.

I would also like to thank the other members of the astronomy group for their freely given support and advice, especially Ljiljana Skuljan who taught me how to use the MRS and also obtained some observations of Sakurai's Object while on her observing runs.

Other people who provided valuable information were Albert Jones with his visual estimates of the magnitude of Sakurai's Object and Martin Asplund with his colours from model C stars.

This piece of research has also made use of the *Simbad* database, operated at CDS Strasbourg, France, and the *Astronomical Data center* and *Astrophysics Data System* abstract service, both provided by NASA. All of these databases were accessed via the World Wide Web.

References

[1] H.W. Duerbeck S Benetti. Sakurai's Object - a possible final helium flash in a planetary nebula nucleus. *ApJ*, 468:L111–L114, September 1996.

[2] I. Iben J.B. Kaler J.W.Truran. On the evolution of those nuclei of planetary nebulae thea undergo a final helium shell flash. *ApJ*, 264:605–612, Jan 1983.

[3] I. Iben. Planetary nebulae and their central stars - origin and evolution. *Physics Reports*, 250:1–94, 1995.

[4] G. Gonzalez D.L. Lambert G. Wallerstein N.K. Rao V.V. Smith J.K. McCathy. FG Sge - a newborn R CrB star. *ApJ suppliment series*, 1998.

[5] G.C. Clayton O. De Marco. The evolution of the final helium flash star V605 Aquilae, from 1917 to 1997. *Astr.J*, 114:2679, Dec 1997.

[6] T.E. Harrison. A near-infrared survey of old novae. ii. CK Vulpeculae and V605 Aquilae. *PASP*, 108:1112–1116, December 1996.

[7] M.S. Bessell. *UBVRI* photometry with a Ga-As photomultiplier. *PASP.*, 88:557–560, August 1976.

[8] A.W.J. Couisns. Circ. South African Astr. Obs., 1983.

[9] H.W. Duerbeck S. Benetti A.Gautschy A.M. van Genderen C. Kemper W. Liller T. Thomas. The final helium flash object Sakurai: Photometric behavior and physical characteristics . *Astron. J*, 114(4), Oct 1997.

[10] M.D. Albrow. Reduction of Mt John échelle spectra using FIGARO. Internal document, UoC dept of Physics and Astronomy., 1994.

[11] W.H.Press S.A. Teukolsky. Search algorithm for weak periodic signals in unevenly spaced data. *Computers in Physics*, 2(6):77, 1988.

[12] P.C. Keenan. Revised spectral classification of the red carbon stars. *PASP*, 105(691):905–910, Sept. 1993.

[13] C. Barnbaum R.P.S. Stone P.C. Keenan. A moderate resolution spectral atlas of carbon stars. *ApJ Suppliment Series*, 105:419–473, Aug 1996.

[14] M. Asplund B.Gustafsson D.L. Lambert N.K. Rao. A stellar endgame - the born-again Sakurai's Object. *A&A*, 321(L17), 1997.

[15] S. Kimeswenger F. Kerber. The distance of Sakurai's Object. *A&A*, 330:L41–L44, 1998.

[16] C.W. Allen. *Astrophysical Quantities*. The Athelone Press, 1986.

[17] Landolt-Börnstein. New Series.

[18] E Costa J.A. Frogel. Carbon stars in the Large Magellanic cloud: Luminosities, colours and implications for the history of star formation. *Astron. J*, 112(6), Dec 1996.

[19] S.R. Pottasch. *Planetary Nebulae*. Reidel, Dordrecht, 1984.

[20] M. Zeilek E.v.P. Smith. *Introductory astronomy and astrophysics*. Saunders College Publishing, second edition, 1987.

[21] T. Kipper V.G. Klochkova. The chemical composition of Sakurai's Object. *A&A*, 324:L65–L68, 1997.

Appendix A

Reduction procedure

This is the reduction procedure followed to convert the images obtained with the MRS into useful numbers. Words in capital letters are Figaro commands or procedures.

A.1 Image preparation

RDFITS reads the fits image into Figaro. IPREP rotates the image 3 times 90°, so that the image is displayed horizontally, with shorter wavelengths to the left. It then removes cosmic rays by calling BCLEAN. This works well on images which do not have many cosmic rays, but may leave some on long exposures with lots of cosmic rays. The performance of BCLEAN can be improved by adjusting the parameters used to recognise the cosmic rays. CLEAN provides an alternate, interactive cosmic ray removal routine which may give better results. IPREP outputs both the rotated and the cleaned images, so the rotated image can be cleaned "by hand", using the routine CLEAN if the automatic BCLEAN was unsatisfactory. The BCLEAN routine also attempts to clean the arc spectrum, sometimes misinterpreting parts of lines as cosmic rays. Typical arc exposure times are not long enough to collect cosmic rays, so as a rule the rotated arcs were used, and the cleaned ones discarded. An example of a raw spectrum is shown in figure A.1.
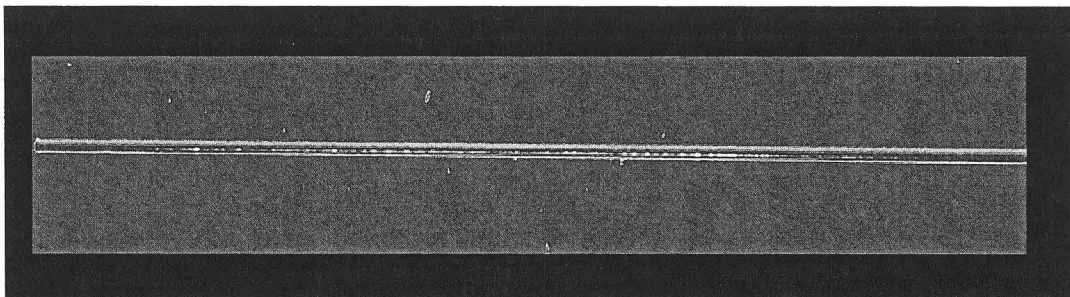
Figure A.1: This raw spectrum has been rotated but has not had the cosmic rays removed.

The spectra were straightened. This step may not be strictly necessary, due to the scrunching of the whole image, however it does simplify extraction and

reduce sky background noise. A polynomial is fitted through the cross-sectional peak of the spectrum, then the columns (perpendicular to the dispersion) are shifted according to that fit to straighten it. If the image is straightened, the arc and flat field must also be straightened using the same polynomial.

A.2   The dispersion solution

Some rows of the arc spectrum are then EXTRACTed. It doesn't really matter how many rows, but remember which they were. This will be the basis of the dispersion solution.

The routine ARC interactively creates a dispersion solution. Most dispersion solutions look something like fig. A.2. Care should be taken that the solution does not do peculiar and unlikely things at the ends, and that stray blends and other oddities do not upset things. The RMS deviation should be kept at about the Å/pixel measurement which changes depending on the grating and order used. Once one good solution has been found for any one wavelength region, it can be used to automatically find lines in a second solution. This speeds the process up remarkably, but does not automate it compleatly. The solution still requires careful inspection.
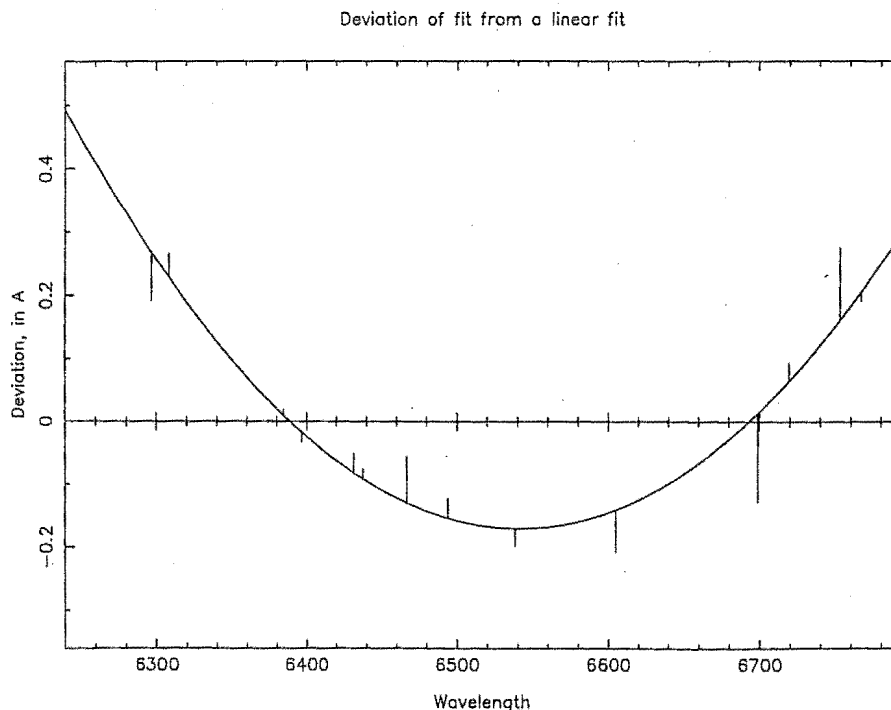

Figure A.2: The deviations from a linear fit in a dispersion solution. Most solutions were similar to this one. Fits which suddenly change in direction especially toward the ends are a sign that something is amiss.

A.3 Scrunching

Scrunching is the term applied to using the dispersion solution to assign wavelength values to the image of the stellar spectrum.

IARC extends the dispersion solution over the entire arc image, assigning each pixel in the arc spectrum a wavelength value, taking into account shifts between rows. This is then used to assign wavelength values to the individual pixels in the image with ISCRUNCH. This step can obviate the need for straightening the image, since each pixel is assigned a wavelength rather than each column. If the unstraightened spectrum is prepared like this and then all the rows containing stellar spectrum extracted, more sky is included than is strictly necessary. The arc spectrum should be ISCRUNCHed, and then inspected for any discontinuities on lines or other odd-looking bits. These can usually be dealt with by varying the prompted parameters when using IARC. Problems well away from the central few rows can be tolerated, as that part of the image is not going to be used, but these regions should be noted and avoided when choosing regions of the image for sky subtraction (see figure A.3.
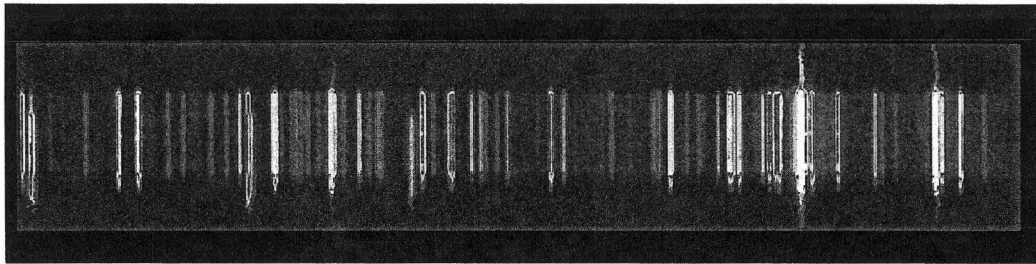
Figure A.3: This scrunched arc spectrum is an indication of an acceptable IARC. The slight deviations at the ends of the more intense lines are all right because they are well away from the part of the spectrum that will be extracted.

A.4 Sky subtraction

The part of the ISCRUNCHed image with the spectrum in it is extracted, usually about 10 rows. Sky subtraction can be done now if necessary. For sky subtraction 10 rows are extracred from the ISCRUNCHed image, away from the stellar spectrum and from any parts which exhibited problems after ISCRUNCHing the arc. If there is serious noise or cosmic rays in this image, repeat 3 times, and use the MEDIAN command, which takes the point by point median of three files. This can also deal with cosmic rays which have not been removed previously. This 1D sky spectrum is subtracted from the 1D stellar spectrum.

The result of these procedures is a one-dimensional wavelength calibrated spectrum, with sky lines subtracted. The fitting of a continuum to this spectrum is complicated by the type of star that has been observed, and is discussed in Chapter 3.